JOURNAL OF GEOPHYSICAL RESEARCH, VOL. 105, NO. D15, PAGES 19,991–20,011, AUGUST 16, 2000

Analysis of residual mean transport in the stratosphere 1. Model description and comparison with satellite data

Hans R. Schneider, Dylan B. A. Jones, and Michael B. McElroy

Department of Earth and Planetary Sciences and Division of Engineering and Applied Sciences

Harvard University, Cambridge, Massachusetts

Guang-Yu Shi

Institute of Atmospheric Physics, Chinese Academy of Sciences,

Beijing, China

Abstract. A coupled two-dimensional model of the dynamics, chemistry, and radiation of the stratosphere is described. The effects of Rossby wave mixing are parameterized by externally specified coefficients K_{yy}, which are used consistently in the zonal mean momentum equation and the diffusion term of the tracer transport equation. Rossby wave mixing is reduced in the tropics. Transport between the tropics and midlatitudes is controlled by advection in the model. It is shown that subtropical tracer gradients [e.g., *Trepte and Hitchman*, 1992; *Randel et al.*, 1993] are produced as a consequence of the difference between advective timescales in the tropics and the diffusive time scale in midlatitudes. In the annual mean, the flow of air is directed from the tropics toward midlatitudes. However, advection between tropics and midlatitudes takes place in both directions at stratospheric altitudes at any given time. Calculated temperatures show some discrepancies with observations in the polar regions. Distributions of long-lived tracers are compared with observations made by instruments aboard the Upper Atmospheric Research Satellite and data from the Atmospheric Trace Molecule Spectroscopy Experiment. Tropical and midlatitude profiles calculated by the model are in reasonable agreement with observations. The sensitivity of calculated temperatures and distributions of long-lived tracers to the choice of large-scale diffusion coefficients, K_{yy}, is shown to be small due to the dual role of K_{yy} in determining diffusive tracer transport and providing a forcing term for the mean circulation [*Holton*, 1986].

1. Introduction

The calculation of transport rates in the stratosphere is subject to many uncertainties. Until recently it was difficult to determine an acceptable level of accuracy for transport rates in the stratosphere. There were few measurements of long-lived tracers and the effects of transport errors on the assessment of ozone perturbations resulting from chlorofluorocarbon (CFC) emissions did not appear to be critically affected by transport errors. Transport is, however, important for perturbations caused by a localized stratospheric source of tracers. A large part of the uncertainties in the assessment of the effects of stratospheric aircraft can be attributed to different rates of transport in different models. Because the need to better understand stratospheric transport was recognized, several measurement campaigns have been carried out in recent years. The Stratospheric Photochemistry Aerosol and Dynamics Experiment, the Airborne Southern Hemisphere Ozone Experiment and Measurements for Assessing the Effects of Stratospheric Aircraft and Stratospheric Tracers of Atmospheric Transport campaign have produced high-quality data on long-lived trace species such as N_2O, CH_4, CO_2, SF_6 and the pseudotracer mean age, which provide fairly stringent constraints on transport rates. Furthermore, the quality of measurements of long-lived tracers at higher altitudes has improved through the observations made by instruments on the Upper Atmospheric Research Satellite

Paper number 2000JD900213.
0148-0227/00/2000JD900213$09.00

(UARS) and on the Space Shuttle based Atmospheric Trace Molecule Spectroscopy Experiment (ATMOS).

The recent measurements have also revealed new characteristics of stratospheric tracer concentrations. Observations of aerosols [*Trepte and Hitchman*, 1992; *McCormick and Veiga*, 1992] and long-lived trace species such as N_2O and H_2O [*Randel et al.*, 1993] have indicated that mixing between the tropics and the midlatitudes is limited. Aircraft measurements of NO_y and O_3 [*Murphy et al.*, 1993] also confirm the existence of an air mass boundary in the subtropics. The mixing barrier manifests itself in fairly steep subtropical gradients of long-lived tracers. The above observations as well as analyses of ozone mixing ratios [*Leovy et al.*, 1985; *Manney et al.*, 1993] show further that episodic irreversible transport out of the tropics occurs during wave events when a pocket or a tongue of tropical air is drawn across the subtropical boundary and subsequently mixed with midlatitude air.

The most useful framework for describing the zonally averaged transport of tracers in the stratosphere is the set of transformed Eulerian mean (TEM) equations (for a review see *Andrews et al.*, [1987]). The zonal mean circulation induced by quasigeostrophic Rossby waves can be calculated analytically for small-amplitude waves in the presence of small dissipation. The stream function for the eddy-induced circulation is given by $v'T'/N^2$ in this case, where v' and T' denote the eddy meridional velocity component and temperature and N^2 the static stability. Using this expression, a residual mean circulation can be defined as the difference between the Eulerian mean circulation and the wave-induced mean circulation. Rewriting the dynamical equations in terms of the residual circulation results in a considerable simplification of the system of equations because the need for the explicit calculation of the contribution of Rossby waves to the zonal mean mass flow is circumvented. The concept of the residual circulation is the theoretical basis for two-dimensional (2-D) models of the stratosphere. The application of a 2-D model for a realistic system entails, however, several implicit and explicit approximations.

The first implicit approximation is associated with the fact that planetary wave amplitudes are finite in the real atmosphere. The equations of motion can still be written in terms of the residual circulation as defined above. The transformed Eulerian equations are exact in the finite amplitude and nongeostrophic case. However, the residual circulation as defined above becomes an approximation of the actual mass flow. To properly describe the transport associated with finite amplitude waves without resorting to a full three-dimensional integration would require invoking the Generalized Lagrangian Mean theory [*Andrews and McIntyre*, 1978] which is not a practical option for performing long-term integrations.

Another approximation, inherent in the 2-D framework is the parameterization of the remaining eddy terms in the set of transformed Eulerian mean equations. For small wave amplitudes or, more precisely, small particle displacements, the eddy flux of a given quantity can be approximated as the product of a diffusion tensor K and the mean gradient of the quantity. The diffusion tensor in the TEM framework is symmetric and has only one significant component K_{yy} in isentropic coordinates [*Tung*, 1986], where y denotes the north-south coordinate following isentropic surfaces.

Explicit assumptions used in 2-D models include the magnitude and the spatial and temporal distribution of K_{yy}, the treatment of the upper and lower boundaries of the stratosphere and parameterizations of other effects like gravity wave drag and vertical mixing. Additional adjustable parameters are used in many current assessment models. Some models, for a variety of reasons, do not attempt to achieve consistency between the advective and diffusive components of transport or heating rates and model ozone.

Due to different approximations incorporated within models, the rates of transport differ considerably between models. This is reflected in model calculated concentrations of long-lived tracers like N_2O [*Park et al*, 1999]. It is, generally, not obvious which assumption or which combination of approximations determines a particular model result.

In this and the following paper we will investigate to what extent the picture of stratospheric transport obtained using conventional residual circulation theory with a minimum of additional assumptions explains the observed distributions of long-lived tracers. In the present paper, we will describe a new coupled 2-D model and compare results for the distribution of long-lived tracers with UARS and ATMOS data. The companion paper will focus on the lower stratosphere and especially on stratospheric concentrations of CO_2 and the distribution of the mean age. The sensitivity of the model results to external parameters will be examined in both papers. We will show that a 2-D model can provide robust explanations for many of the observed features of the distributions of long-lived tracers and the mean age of stratospheric air.

The 2-D model and the choices for the external parameters will be described in section 2. The model consists of a dynamics module which includes the nonlinear zonal mean momentum advection terms, a comprehensive chemistry module and a radiative transfer scheme for the calculation of heating rates. The modules are coupled. The heating rates which drive the dynamics are calculated using model ozone and model temperatures. The following parameters are specified externally: (1) mesospheric drag which is necessary to close the polar night jets, (2) the distribution of eddy diffusion coefficients K_{yy} to parameterize Rossby wave diffusion on isentropic surfaces, (3) the tropospheric heating rates, and (4) coefficients K_{zz} to describe vertical diffusion in the troposphere and stratosphere. The coefficients K_{yy} determine the eddy flux of potential vorticity

as well as the diffusive component of the tracer transport. Therefore advective and diffusive transport are consistent with each other in the model. No attempt has been made to modify the diffusion coefficients for tracers with different lifetimes or otherwise account for chemical eddies.

In section 3, model results for dynamical variables will be discussed. While the model reproduces the general structure of zonal mean wind and temperature distributions in the stratosphere, there are discrepancies between calculated fields and observations. Stratospheric polar temperatures are too warm in the winter hemisphere and too cold in the summer hemisphere. It is shown that zonal wind and temperature distributions depend only weakly on the assumption for K_{yy}. The mean meridional flow in the subtropics is characterized by seasonally varying outflow from and inflow in the tropical regions.

Distributions of long-lived tracers are compared with UARS and ATMOS data in section 4. It is shown that the calculated tropical and midlatitude profiles of long-lived tracers are in reasonable agreement with satellite observations. Distributions of long-lived tracers do not depend strongly on the choice of K_{yy} because eddy diffusion acts both to flatten the slopes of isolines of tracers and to intensify the residual circulation which partially restores the tracer gradients [*Holton*, 1986]. It is shown further that subtropical tracer gradients are generated as a natural consequence of the difference between the timescale for advection in the tropics and the timescale for diffusion in the extratropics. The location and the steepness of the gradients are modulated by changes in the tropical circulation resulting, for example, from the quasi-biennial oscillation (QBO) [*Jones et al.*, 1998].

Model results depend to a large extent on build-in assumptions about the effects of unresolved physical processes. The most important factors that determine the results of our model are (1) quasi-horizontal diffusion is acting in mid and high latitudes only. The magnitude of the diffusion coefficients decreases smoothly toward the subtropics. Transport within the tropics and across the subtropics is completely advective in nature and consistent, within the TEM framework, with the large-scale diffusion specified in the extratropics. (2) The nonlinear momentum advection terms are included in the dynamics module and have a significant effect on the circulation in the vicinity of the equator [*Jones et al.*, 1998]. (3) Frictional drag in the lower stratosphere is assumed to be small except for the region immediately above the tropopause.

2. Model Description

The model consists of four coupled modules for the dynamics, radiation, chemistry, and the transport. The circulation and temperatures are determined by heating rates which are calculated using the model ozone and model temperatures at the previous time step. Wave mixing is not explicitly calculated. However, the circulation and the advective transport are consistent in the model. The assumed eddy mixing coefficients are used in the diffusion term of the tracer transport equations and also in the zonal mean momentum equation to describe the eddy potential vorticity flux [cf. *Holton*, 1986].

Log (pressure) coordinates are used in the vertical. All results were obtained with a horizontal resolution of 5° and a vertical resolution of 2 km. A staggered grid is used. The center of the lowest grid box is located at 1 km in altitude, the upper boundary is at the height of 81 km.

2.1. Dynamical Model

The dynamical integrator is based on the model described by *Schneider and Geller* [1985]. Versions of it have also been used in conjunction with other chemistry transport models [*Schneider et al.*, 1989; *Hou et al.*, 1991; *Ko et al.*, 1993; *Schneider et al.*, 1993]. The model includes the nonlinear zonal mean momentum advection terms. Zonal mean winds are specified at the lower boundary (1 km), using climatological values based on *Oort* [1983]. A rigid lid is placed at the upper boundary. The equations used are listed in Appendix A. Externally specified parameters are described as follows.

2.1.1. Zonal mean forcing by gravity waves. The breaking of gravity waves at mesospheric levels results in a strong deceleration of the mean flow and is responsible for closing the polar night jets at high altitudes. In the winter hemisphere the divergence of the Eliassen-Palm flux due to planetary waves leads to additional mean flow deceleration. While the relative importance of planetary and gravity waves in the winter hemisphere is uncertain, the closure of the easterly summer jet at mesospheric levels has to be achieved by gravity wave drag alone. Furthermore, gravity wave breaking in the vicinity of the tropopause has an impact on the circulation of the lower stratosphere.

The effects of breaking gravity waves are incorporated into our model in the form of a Rayleigh friction parameterization. This is an oversimplified description of gravity wave induced drag. However, little is known about the spectrum and amplitudes of gravity waves emanating from the troposphere. Therefore explicit gravity wave breaking parameterizations have to assume a spectrum and assign amplitudes to each gravity wave which results in a large number of adjustable parameters.

The friction profile is assumed to vary with height only, we do not attempt any modulation as a function of latitude. Except for the altitude region between 10 and 30 km, the vertical profile is taken to be

$$\beta_r(z) = b_1 + b_2 \tanh((z - 70)/8),$$

similar to *Holton and Wehrbein* [1980]. The variable z

denotes the pressure altitude in units of kilometers, b_1 is set to $1/30$ day^{-1}, and b_2 is $1/.8$ day^{-1} which results in a damping timescale of about 20 days at 40 km and a deep sponge layer with a damping timescale smaller than a day at 80 km.

The value of b_2 is chosen to ensure closure of the polar night jets. The 30 day damping timescale at low altitudes, b_1, is determined as part of the heating parameterization used in the troposphere as discussed below. Between 10 and 30 km altitude, the mechanical damping is reduced substantially. Damping timescales increase from 30 days to about 90 days within 5 km above the midlatitude tropopause and are larger than a season for the region between 15 and 25 km with a maximum of 300 days at 20 km. Between 25 and 30 km the friction parameter increases again to match the profile given by the above equation.

Our assumption that gravity wave induced drag is significant near the tropopause but reduced for the remainder of the lower stratosphere was motivated by model studies of planetary wave propagation and earlier results for tracers [*Hou et al.*, 1991]. It is shown in the companion paper [*Schneider et al.*, this issue] that modeled tracer distributions exhibit a strong sensitivity to the frictional damping specified in the lower stratosphere. However, the vertical resolution of the current model version does not allow the use of detailed assumptions about the vertical structure of the momentum deposition by gravity waves. Therefore the sensitivity of model results to the prescription of gravity wave induced drag in the lower stratosphere will be further investigated in a version of the model with higher vertical resolution and will be reported seperately.

2.1.2. Large-scale eddy diffusion coefficients K_{yy}. The distribution of Rossby wave mixing coefficients K_{yy} is one of the most important parameters for a 2-D model. The coefficients depend on the planetary wave field in the stratosphere which is a function of the forcing of planetary waves in the troposphere and their upward propagation through the mean zonal winds. A planetary wave parameterization was developed by Garcia [1991]. It was applied to stratospheric circulation statistics by *Randel and Garcia* [1994]. The model of *Bachmeister et al.* [1995] also uses calculated planetary waves to derive the zonal mean mixing coefficients. However, mixing in the lowermost stratosphere is partly due to synoptic-scale waves which are not accounted for in planetary wave parameterizations. Because of this uncertainty and because our main interest is in understanding the sensitivity or robustness of our model results, we use externally specified mixing coefficients. We will compare results for three different distributions of diffusion coefficients.

The first set of coefficients K_{yy} used is based on the results of an analysis of circulation data by *Newman and Schoeberl* [1986] and *Newman et al.* [1988]. The analysis showed large values of K_{yy} in the regions of the polar night jet cores in winter. Another, smaller maximum was diagnosed to occur in the lower stratosphere above the tropospheric jets during spring and summer. The maximum values of the coefficients are several 10^6 m^2 s^{-1}. Given the difficulties encountered in determining large-scale mixing coefficients from data, we utilize only the information about the location, the timing and the approximate amplitude of the maxima.

The distribution of K_{yy} used in the model is shown in Figure 1 for each season. Regions of large K_{yy} are assumed to be centered around 60 km in altitude and 70° latitude in winter and 18 km and 45° in summer. The spatial distribution of K_{yy} is specified by assuming an exponential decay away from the maxima to a background value of 0.5×10^5 m^2 s^{-1} in mid and high latitudes. The diffusion coefficients are reduced gradually toward the subtropics. Equatorward of 15° the value of K_{yy} is set to 10^4 m^2 s^{-1}. The upper maxima grow and decay sinusoidally in time, reaching peak values in midwinter. The lower stratospheric maxima are 180 days out of phase with the upper maxima, peaking at the beginning of July.

While the high-altitude maxima in winter result from upward propagating planetary waves interacting with the zonal mean flow, the low-altitude mixing may result from planetary waves trapped by the summer easterlies and the effects of mesoscale waves. Because there are no reliable estimates for the values of the diffusion coefficients at low altitude, the lower stratospheric maxima are assumed to be of the same magnitude in both hemispheres. The values at higher altitudes are lower in the Southern Hemisphere compared to the Northern Hemisphere to account for the difference in the structure of planetary waves in the hemispheres. The pattern of K_{yy} reflects broadly the fact that large-amplitude planetary waves propagate to high altitudes in winter and that waves of smaller amplitude in summer are trapped at low altitudes by the easterly zonal winds in the stratosphere.

The distribution also reflects the fact that weak zonal winds at low latitudes prevent large amounts of planetary wave activity from reaching the tropics. Negligible quasi-horizontal mixing in the tropics produces a "tropical pipe" [*Plumb*, 1996] in the model. However, the walls of the "pipe" are not sharply defined and, during solstice conditions, the "pipe" is open on the summer side. The assumed spatial distribution of K_{yy} is such that diffusive transport through the subtropics is generally an order of magnitude smaller than the advective transport by the residual circulation in the model. The distribution of K_{yy} shown in Figure 1 will be referred to as the low-K_{yy} case in the following.

The second set of eddy mixing coefficients used for the model runs discussed in the following sections is obtained by multiplying the distribution of the low-K_{yy} case by a factor of 2, except in the tropics where the values are kept the same, at 10^4 m^2 s^{-1}. This parameter setting will be referred to as the large-K_{yy} case in the following. Runs in which only the K_{yy} in the up-

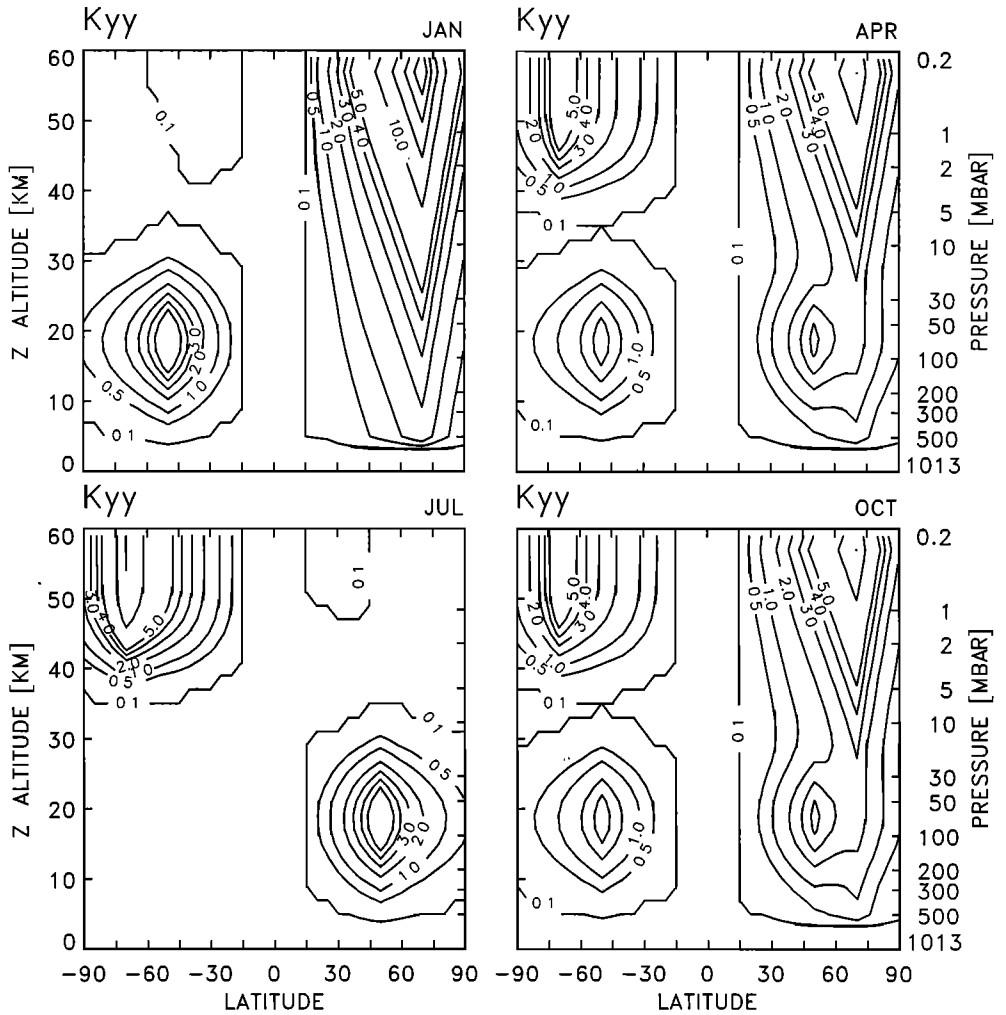

Figure 1. Distribution of K_{yy} for the low-K_{yy} case (see text) for the four seasons. Units are 10^5 m s^{-2}.

per stratosphere or the lower stratosphere were doubled have also been made. However, these runs do not provide significantly more information than the case where K_{yy} is doubled everywhere in the extratropics.

In order to check to what extent the assumed seasonal dependence of the extratropical mixing determines the seasonality of tracer distributions obtained in the model, control runs have been made with a constant-K_{yy} case with the diffusion coefficients set to a constant 3. $\times$ 10^5 m^2 s^{-1} in mid and high latitudes of both hemispheres, independent of season. Tropical values and the gradual reduction of K_{yy} through the subtropics are the same as in the other cases.

2.1.3. Parameterization of tropospheric heating rates. No attempt is made to describe the troposphere in a consistent manner. The requirements for the model troposphere are that it has to allow the correct mass flux into and out of the stratosphere and that its temperatures are reasonably close to observed values in order to allow the calculation of infrared radiative fluxes in the stratosphere. To force the tropospheric temperatures to be close to climatological values, heating rates are prescribed in the troposphere.

The parameterization used in the model is adopted from *Cunnold et al.* [1975]. Some modifications have been made to the scheme to account for interhemispheric asymmetries. The heating rates are specified as

$$\bar{Q}(y,z,t) = \alpha(z)(\bar{T}(y,z,t) - \bar{T}^*(y,z,t)),$$

where y and z are the horizontal and vertical coordinates and t is the time of the year. $\bar{T}$ is the actual model temperature at a given time step and $\bar{T}^*$ represents an equilibrium temperature as defined by *Cunnold et al.* [1975]. Variable α is a time invariant relaxation coefficient.

In addition, a frictional damping with a timescale of 30 days is prescribed in the model troposphere. This parameter ensures that there will always be a finite mean meridional heat flux in the model troposphere and that heating rates will remain be finite. The model temperatures, therefore, cannot become equal to the equilibrium temperatures $\bar{T}^*$. The meridional overturning in the troposphere, calculated using this parameterization, agrees qualitatively with the mass flux diagnosed by *Plumb and Mahlman* [1987] from the Geophysical

Fluid Dynamics Laboratory (GFDL) general circulation model.

2.1.4. Vertical diffusion. Coefficients for vertical mixing in the troposphere are chosen to give a vertical exchange time of about 1 month throughout the height of the troposphere. We assume that vertical mixing in the stratosphere is 2 orders of magnitude smaller. The value of the coefficient used is 0.1 m^2 s^{-1} in the stratosphere and 10 m^2 s^{-1} in the troposphere.

For numerical reasons, the mixing coefficients cannot be specified as a step function with the changeover from tropospheric to stratospheric values occurring in the layer closest to the tropopause. Therefore the effective tropopause height is not a well-defined quantity in the present model with its coarse vertical resolution of 2 km. Mid- and high-latitude ozone profiles in the vicinity of the tropopause and, consequently, ozone columns have to be interpreted with caution. Ozone profiles in the tropics are not very sensitive to the vertical diffusion because the general motion is upward and no accumulation of ozone occurs above the tropopause. However, the propagation of seasonally varying tracer signals, such as concentrations of CO_2, into the stratosphere is affected by the vertical diffusion in the tropopause layer and the lowest layer of the stratosphere. Using the bottom or the top of the tropopause layer as the reference height results in substantial differences in computed attenuation rates. Model calculated attenuation rates for the seasonal fluctuations of CO_2 in the stratosphere agree with observations if amplitudes are normalized to the bottom of the tropopause layer. The propagation of time dependent tracer signals is examined in detail by *Kogan-Le Flore* [1999].

2.2. Radiative Transfer Model

Radiative heating is calculated with a version of the model described by *Shi* [1981, 1984]. An exponential sum fitting technique is used to calculate infrared radiative transfer. Calculated profiles agree well with line-by-line models as shown by the comparison with the GFDL model in Figure 2. The *Lacis and Hansen* [1974] parameterization is used for the shortwave fluxes.

Heating rates are calculated for every latitude based on model ozone and the model-generated temperature profile. The heating rates calculated for tropospheric altitudes are not used; they are replaced by the parameterization described above. There is, necessarily, a transition region where calculated and parameterized heating rates are matched. This region is in the lower stratosphere, and the upward transport of tracer material in the tropics from the troposphere into the stratosphere is sensitive to the height at which the tropospheric parameterization is cut off and the depth of the cutoff region. Therefore no attempt has been made to account for the effects of high clouds or varying albedo, for example. For all calculations shown in this paper, clear-sky conditions are assumed and the surface albedo is set to 0.3. We will discuss the sensitivity to the matching of heating rates at the tropopause level in the companion paper in conjunction with the simulations of CO_2 and N_2O in the lower stratosphere. The initial tuning in our model was performed to obtain a reasonable representation of the temperature distribution near the tropical tropopause.

Above 60 km, only solar heating rates are calculated. The infrared flux divergence is approximated as

$$Q_{IR} = -\langle Q_{\text{solar}} \rangle - \alpha(z)(T(z) - T_{\text{std}}(z))$$

where $\langle Q_{\text{solar}} \rangle$ denotes the global average of the solar heating, $\alpha(z)$ is a fixed radiative relaxation coefficient and T_{std} the standard atmosphere temperature profile.

To avoid the need to recompute the heating at every dynamical time step, the functional derivative of the radiative heating rates with respect to temperature is calculated periodically. For every latitude we define a matrix

$$\alpha(z, z') = \delta Q(T(z))/\delta T_c(z'),$$

where $\delta T_c(z')$ is a function that has a finite value only at z'. For the determination of α in finite differences, a function with a narrow compact support centered at z' is used. If heating rates $Q_o(z) = Q(T_o(z))$ are known for a temperature profile T_o, the heating for a temperature $T(z)$ can be expressed as

$$Q(T(z)) = Q_o(z) + \int dz' \alpha(z, z')(T(z') - T_o(z')).$$

New heating rates are calculated every 5 to 10 days during a model integration. The calculation of the matrix α is computationally intensive as it requires as many radiative transfer calculations as there are vertical levels. However, we found that our model results for tracers do not change significantly if α is recomputed every 90 days only or even if an annual average of the matrix is used.

2.3. Chemistry Model

The chemistry module is a newly developed family model and includes a comprehensive set of reactions for the chemistry of the stratosphere. Long-lived species and families are transported. Short-lived species are assumed to be in photochemical equilibrium. The steady state equations are solved every 5 to 10 days using the Newton-Raphson method. Production terms and loss frequencies for the long-lived species are recomputed at the same time interval. The model solves for 24 hour average concentrations by using diurnal coefficients which are determined periodically by performing a forward integration through 1 day.

Photodissociation rates are computed using the radiative transfer code of the Harvard Photochemical model [*Salawitch et al.*, 1994] with the Schumann-Runge Bands treated as described by *Minschwaner et al.* [1992]. Cross sections have been updated following *DeMore et al.* [1997]. Details of the model are given in Appendix

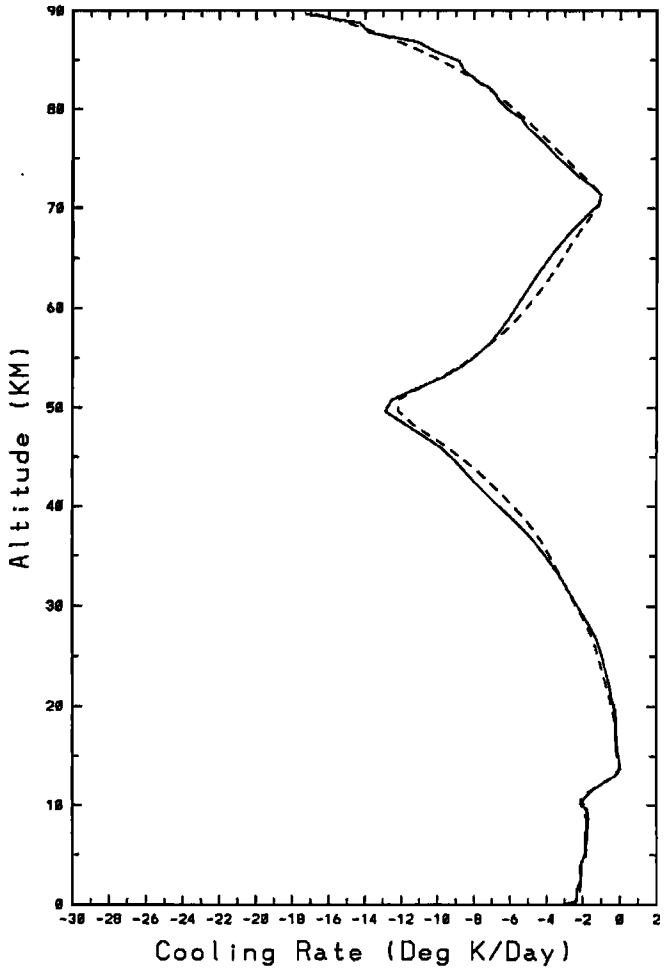

Figure 2. Infrared heating rates calculated by the radiation model (solid line) compared to results of the GFDL radiative transfer code (dashed line) for specified profiles of temperature, H_2O, CO_2 and O_3.

B. A chemical integrator test has been performed, and results can be found in the NASA/Langley database for the Models and Measurements Intercomparison Workshop II.

2.4. Transport Model

Advection of long-lived tracers is computed using a fourth-order version of the Square Root Scheme [*Schneider*, 1984]. This scheme is fairly accurate and has small internal diffusion and dispersion. The diffusive component of the transport of long-lived tracers is treated as a diffusion along isentropes with the same coefficients K_{yy} that are used in the dynamics module. The diffusion tensor has only one significant component in isentropic coordinates [e.g., *Tung*, 1986]. The components of the tensor in pressure coordinates are determined by rotating the tensor in isentropic coordinates by the angle formed by the intersection of potential temperature and pressure surfaces. This angle is determined at every grid point and time step using the model-calculated temperatures. The coordinate rotation produces nonzero values for the components K_{yz} and K_{zz}. The coefficients assumed for the background vertical mixing in the troposphere and stratosphere as described above are added to the component K_{zz} determined by the rotation of the tensor into pressure coordinates.

3. Model Circulation

The lower boundary condition for the dynamics consists of specified zonal mean winds at approximately 1 km as a function of the time of the year. Winds have been taken from the climatology of *Oort* [1983]. For chemical tracers, surface concentrations or fluxes are prescribed where appropriate. Initial conditions for a model run are a barotropic zonal mean wind field obtained by setting the zonal wind to its lower boundary value at every altitude. Initial temperatures are calculated to satisfy thermal wind balance. Heating rates are calculated for climatological temperatures and a latitudinally constant ozone distribution whose vertical profile is given by the *Krueger and Minzner* [1976] model. The dynamics is allowed to spin up from this state for about 10 days. After the spinup period, chemistry and transport are started and heating rates are recalculated

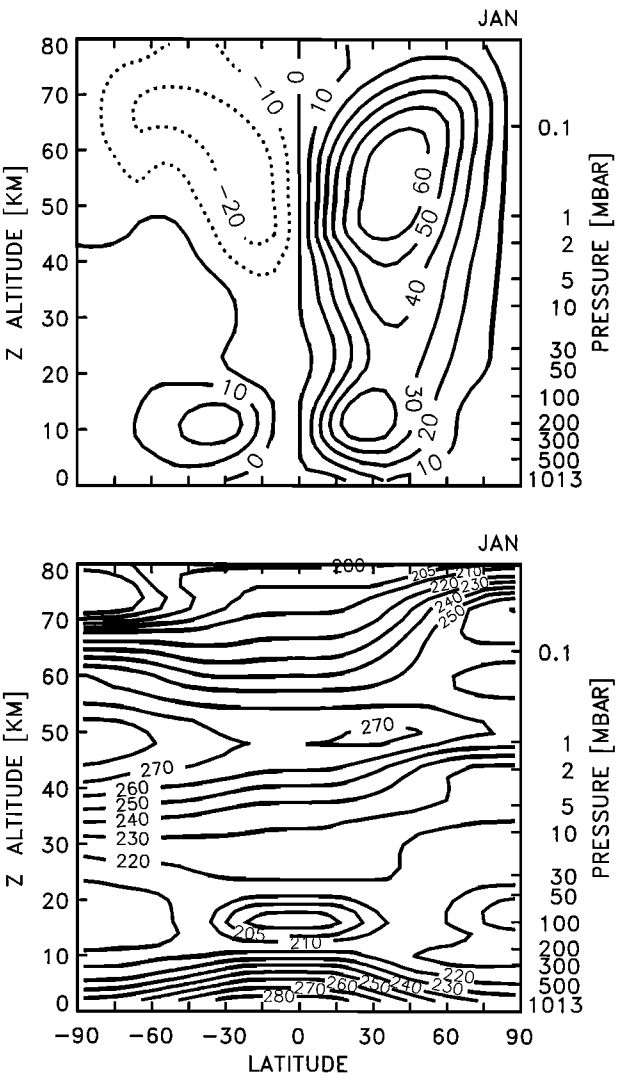

Figure 3. (a) Calculated zonal mean winds (m s^{-1}) and (b) temperatures for January.

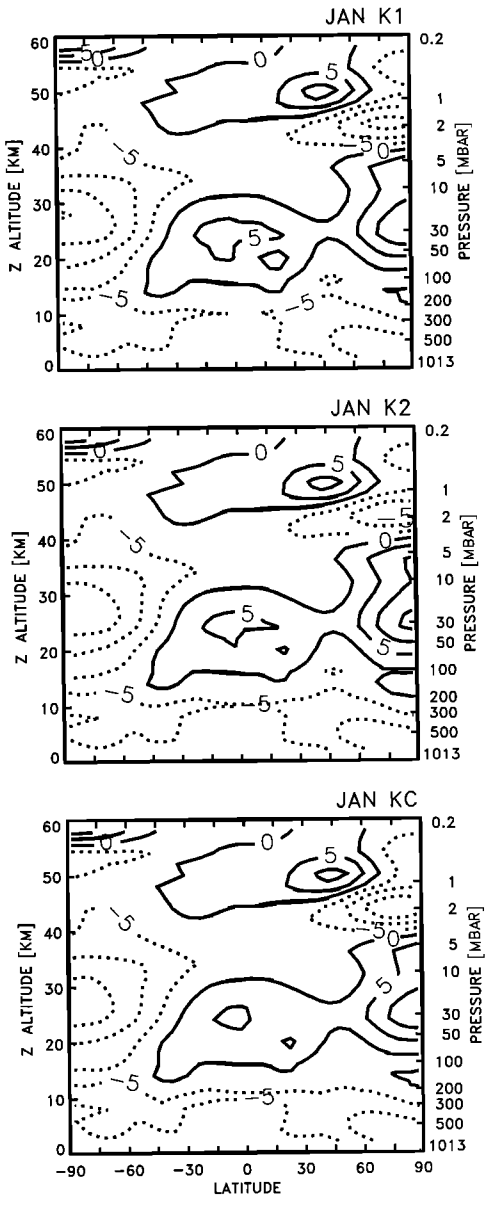

Figure 4. Differences between calculated zonal mean temperatures and observed four-year average temperatures (1978–1982) for January. K1 is for the low-K_{yy} case, K2 is for the large-K_{yy} case, and KC is the difference for the constant-K_{yy} case (see text).

every 5 days, using the model temperatures and model ozone.

Zonal mean winds and temperatures for January, obtained after 3 years of integration, are shown in Figure 3. The structure of the zonal jets agrees fairly well with observations except for the polar regions between 20 and 40 km in altitude. A problem is noticeble in the summer hemisphere. The tropospheric westerlies extend too far into the stratosphere. Accordingly, the summer polar regions are colder and the winter poles warmer than indicated by observations. The easterly summer jet is too weak in comparison with observations.

Model temperatures are compared to the 4-year (1978-1982) average of the temperatures obtained in the analysis of *Wu et al.* [1984] in Figure 4. The three panels show the temperature differences for the three choices of Rossby wave diffusion coefficients K_{yy}, described above for January conditions. The temperature field shows only a weak sensitivity to K_{yy}. In all cases, tropical temperatures are up to 5 K warmer than observations between 20 and 25 km, the winter polar regions between 20 and 40 km are also 5 K too warm for the most part. The temperature difference exceeds 10 K in small areas near the pole. The summer pole is 10 to 15 K too cold in the same altitude region.

Due to the interactive nature of the model, it is difficult to pinpoint a single cause for the deviations of the temperature from observed values. Ozone concentrations compare well with observations above 20 km [*Park et al.*, 1999]. Clearly, we have used simple-minded parameterizations of the physics, and we have

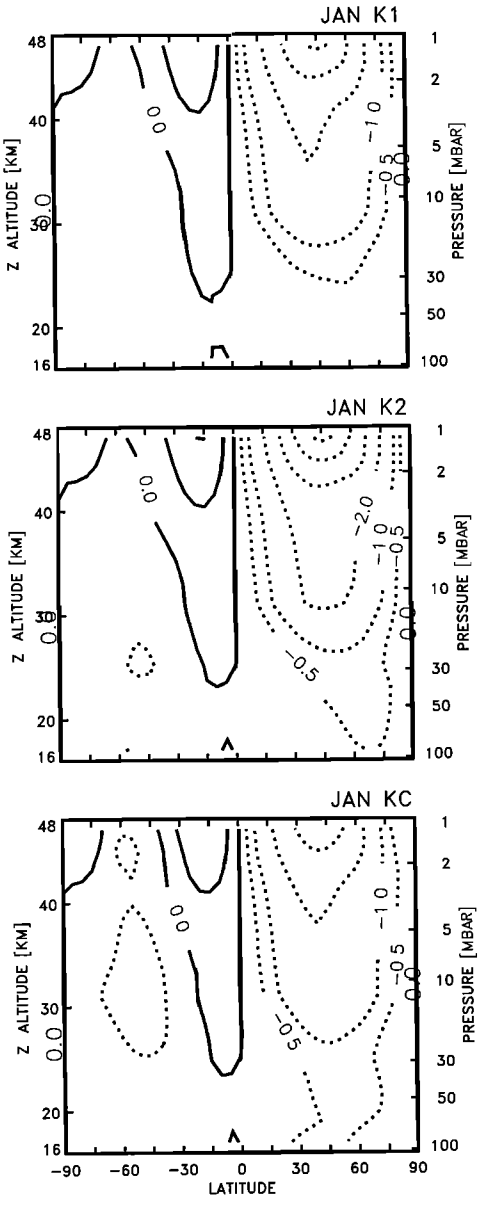

Figure 5. Calculated January zonal mean forcing in units of m s^{-1} d^{-1} for the low-K_{yy} case, K1, the large-K_{yy} case, K2, and the constant-K_{yy} case, KC.

not attempted to simulate the polar regions realistically. It should also be noted that the model predicts the full temperature (see Appendix A), not only deviations from a global mean standard temperature.

The zonal mean forcing terms for the low- and high-diffusion case as well as the control case with constant K_{yy} are shown in Figure 5. Zonal mean accelerations determined from observations are shown in Figure 3 of *Holton et al.* [1995]. The model values agree qualitatively with this analysis; the large K_{yy} case is, perhaps, closest to the observations. In the model the eddy potential vorticity flux $K_{yy}\bar{q}_y$, is responsible for approximately 50% of the total zonal mean forcing above 30 km. The eddy contribution is shown in Figure 6. The remaining half of the zonal acceleration is due to Rayleigh drag.

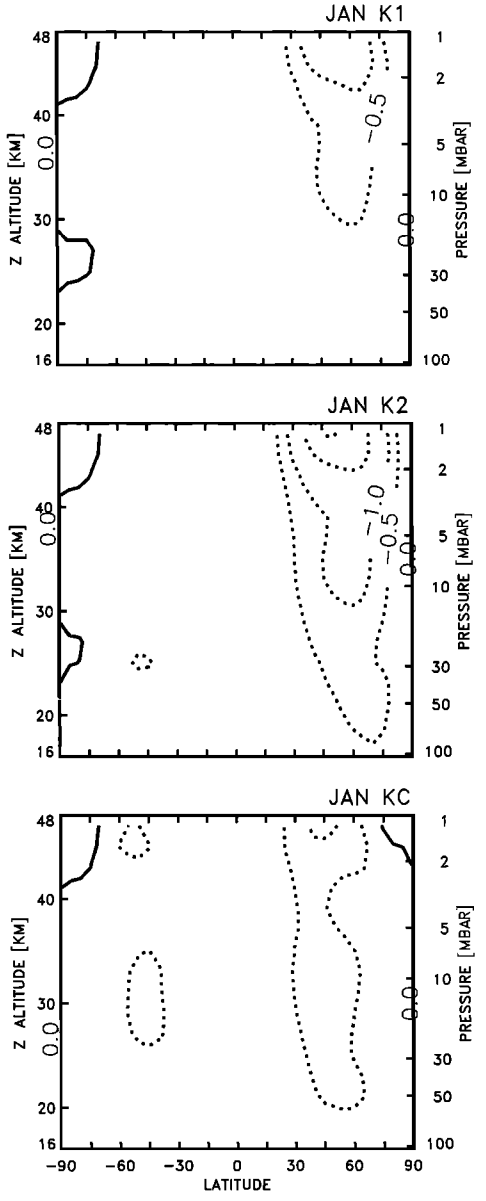

Figure 6. Contribution of the eddy potential vorticity flux to the calculated January zonal mean forcing for the low-K_{yy} case, K1, the large-K_{yy} case, K2, and the constant-K_{yy} case, KC. Units are m s^{-1} d^{-1}.

Meridional mass stream functions for four seasons are shown in Figure 7. Although, in the annual mean sense, the residual mean mass flow is always directed from the tropics to the midlatitudes, inflow into the tropics occurs seasonally at altitudes above 15 km. During solstice conditions, the inflow occurs on the summer side. The pattern is more complicated and rapidly varying during seasonal changeovers.

Calculated horizontal velocity components are shown in Figure 8. The magnitude of the north-south component of the velocity is of the order of 0.1 m s^{-1} or less than 10° latitude per season at midstratospheric altitudes in the tropics and subtropics. Since the flow reverses from summer to winter, advection by the residual mean circulation will not move a parcel, located initially at the equator, into midlatitudes within one season. Correspondingly, a parcel advected into the tropics from midlatitudes may not penetrate deep into the tropics within one season. Horizontal velocities increase with altitude, and the seasonal excursions of parcels become larger correspondingly.

Since no assumptions about horizontal mixing in the tropics are made, the model generates horizontal tracer gradients in that region. The gradients are strongest at low altitudes above the tropopause level where air is subjected to differential vertical advection and only small horizontal movements. The upward motion of a parcel is slow at low altitudes in the tropics. As will be discussed in the companion paper, the mean age of stratospheric air increases by about 2 years within a few kilometers above the tropopause. Therefore a parcel experiences several seasonal reversals of its horizontal velocity component as it ascends across a small-altitude range. Under these conditions, the vertical diffusion assumed to take place in the stratosphere plays an important role in reducing horizontal gradients with altitude. The role of vertical diffusion is examined in greater detail in *Kogan* [1999]. It is also shown there that the present 2 km vertical resolution in combination with the profile used for the vertical diffusion coefficients gives an adequate numerical solution for an upward propagating tracer signal.

4. Comparison of Concentrations of Long-Lived Tracers with Satellite Data

To check the model generated circulation quantitatively, measured distributions of long-lived tracers are compared with model calculated concentrations. Figure 9a compares the model N_2O for November of 1992 with the Cryogenic Limb Array Etalon Spectrometer (CLAES) measurement of N_2O for the same time period. Figures 9b and 9c show model concentrations of CH_4 and CFC-12 together with the measurements by the CLAES instrument for October of 1992. We will limit the discussion to long-lived tracers. Results for ozone and short-lived chemical constituents can be found in the report of the NASA Models and Measurements Intercomparison Workshop II (*Park et al.*, 1999).

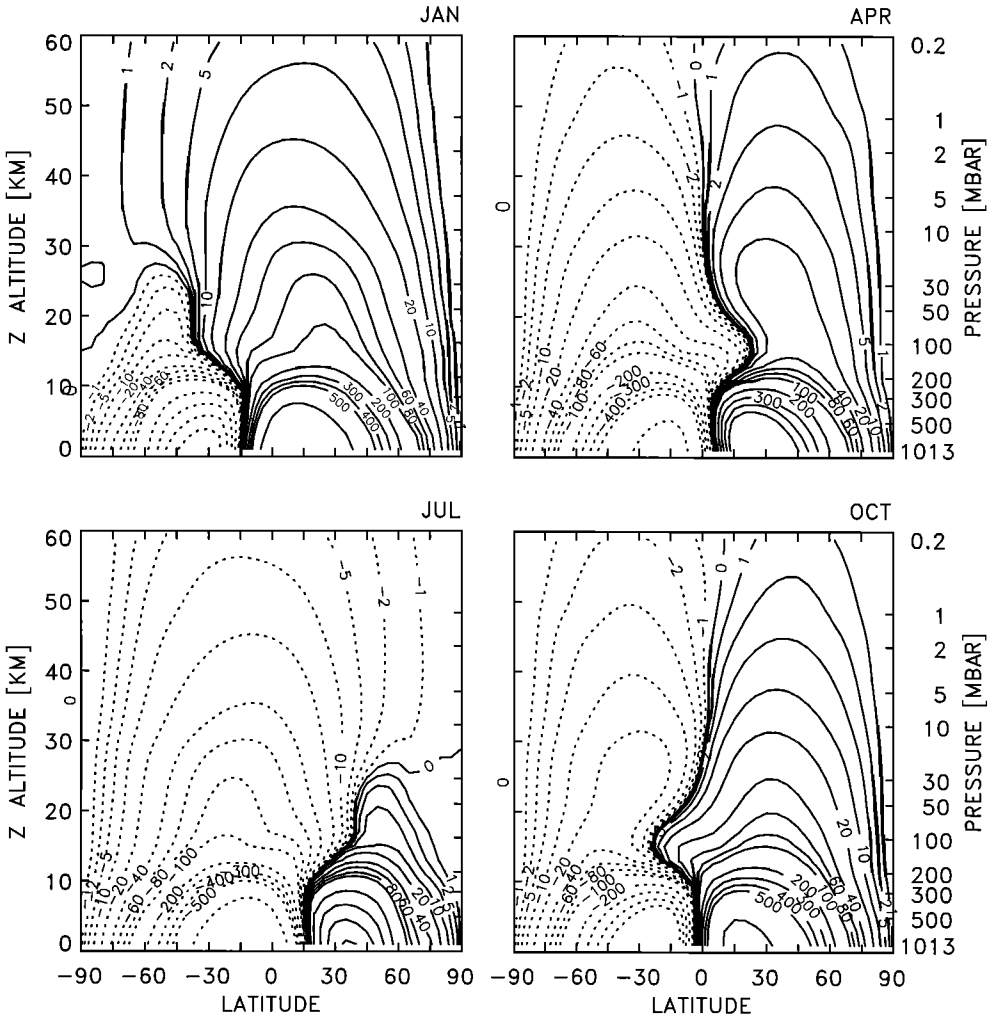

Figure 7. Mean meridional stream functions for the seasons. Units are $m^2\ s^{-1}$. Numerical values are the meridional mass flux scaled by $2\pi a\rho_s$, where a is the Earth radius and $\rho_s \approx 1.3$ kg m^3 is the surface air density.

The results shown in this document are for a model run corresponding to the low-K_{yy} case, except that heterogeneous reactions were included. Heterogeneous chemistry is omitted in the runs presented in this paper as the feedback from ozone losses associated with reactions on aerosols on transport is small. Without heterogeneous chemistry, differences in ozone are less than 10% at altitudes above 20 km. Below 20 km, the differences are larger but result in only small differences in calculated heating rates.

The subtropical tracer gradients produced by the model are not as steep as in the observations and the observed gradients appear further poleward than in the model. The model simulation by necessity represents an average year, the measurements shown are for a particular month. Several important processes are not included in the current version of the model. Concentrations of long-lived tracers are affected by the semiannual oscillation at high altitudes and the quasi-biennial oscillation (QBO) in the lower and middle stratosphere. The effect of the mean meridional circulation associated with the QBO has been studied by *Jones et al.* (1998) in a version of the model which includes the momentum deposition in the tropics by Kelvin and Rossby-Gravity waves that gives rise to the QBO. The QBO modulates the flow into the subtropical regions significantly. Calculated concentrations of N_2O in fall are compared for years when the QBO is in its easterly or westerly phase in Figure 10. Subtropical gradients are enhanced at altitudes where the QBO circulation intensifies the flow towards midlatitudes and the gradients in N_2O, produced by the model, show a pattern that is closer to observations.

Since the eddy diffusion coefficients K_{yy} are reduced gradually toward the subtropics, the subtropical barrier in the model is not fixed at a given latitude but is located wherever the timescale for midlatitude diffusion becomes small compared to the timescale for advection in the tropics. The change in location and steepness of the tracer gradients shown above is a function of the strength of the tropical circulation. Similar effects could result from interannual variations in planetary wave ac-

tivity which has not been taken into account in this version of the model.

The calculated distributions of N_2O exhibit only a weak sensitivity to the specified distribution of K_{yy}. Figure 11a compares N_2O obtained for the large-K_{yy} case with the concentrations for the low-K_{yy} case, shown in Figure 9a. The large-K_{yy} case gives a somewhat better agreement with observations at high latitudes. The low-K_{yy} case is compared with the constant-K_{yy} case in Figure 11b. Increasing K_{yy} tends to decrease the slopes of the isolines of tracers. However, it also has the effect of intensifying the residual circulation which, in turn, leads to steeper slopes. In addition, ozone concentrations and therefore heating rates are altered which gives rise to a small negative feedback effect on circulation changes. The partial cancellation between the slope-steepening and slope-flattening effect of K_{yy} has been examined by *Holton* (1986) in a quasigeostrophic model.

The atmospheric lifetimes of N_2O are almost unaffected by changes in the eddy mixing within the range covered by our choices of K_{yy}. The annual mean atmospheric lifetimes for the small- and large-K_{yy} cases are 127.14 and 126.95 years, respectively, the stratospheric lifetimes are 127.80 and 127.62 years, and the global burdens of N_2O are calculated to be 2.35×10^3 and 2.36×10^3 Tg.

Figure 12 shows a comparison of tropical profiles of N_2O, CH_4, CFC-11 and CFC-12 measured by ATMOS for November of 1994 with model results from the low-K_{yy} case. The ATMOS measurements were taken at 14° N latitude. Model-calculated profiles represent averages between 5° and 15° N. Two additional profiles for N_2O concentrations averaged between ±10° and 15° and 20° N are shown in Figure 12a]. In all cases the model seems to overestimate the abundance of the tracers in the tropics. Agreement with the ATMOS data is, however, reasonable for profiles of the same species averaged over midlatitudes as shown in Figure 13.

In order to investigate the discrepancy between the low-latitude ATMOS data and the model, correlations between N_2O and CFC-11 for the tropics and midlati-

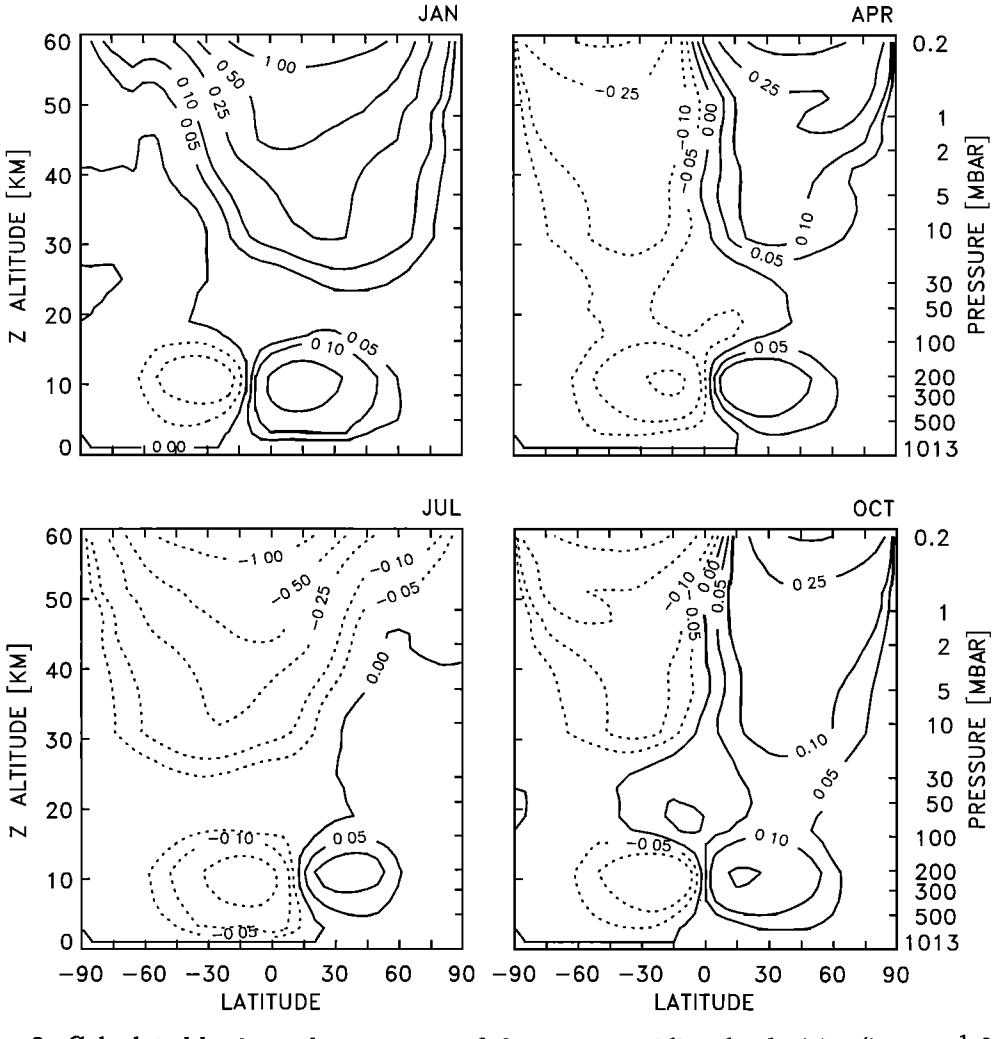

Figure 8. Calculated horizontal component of the mean meridional velocities (in m s^{-1} for the seasons.

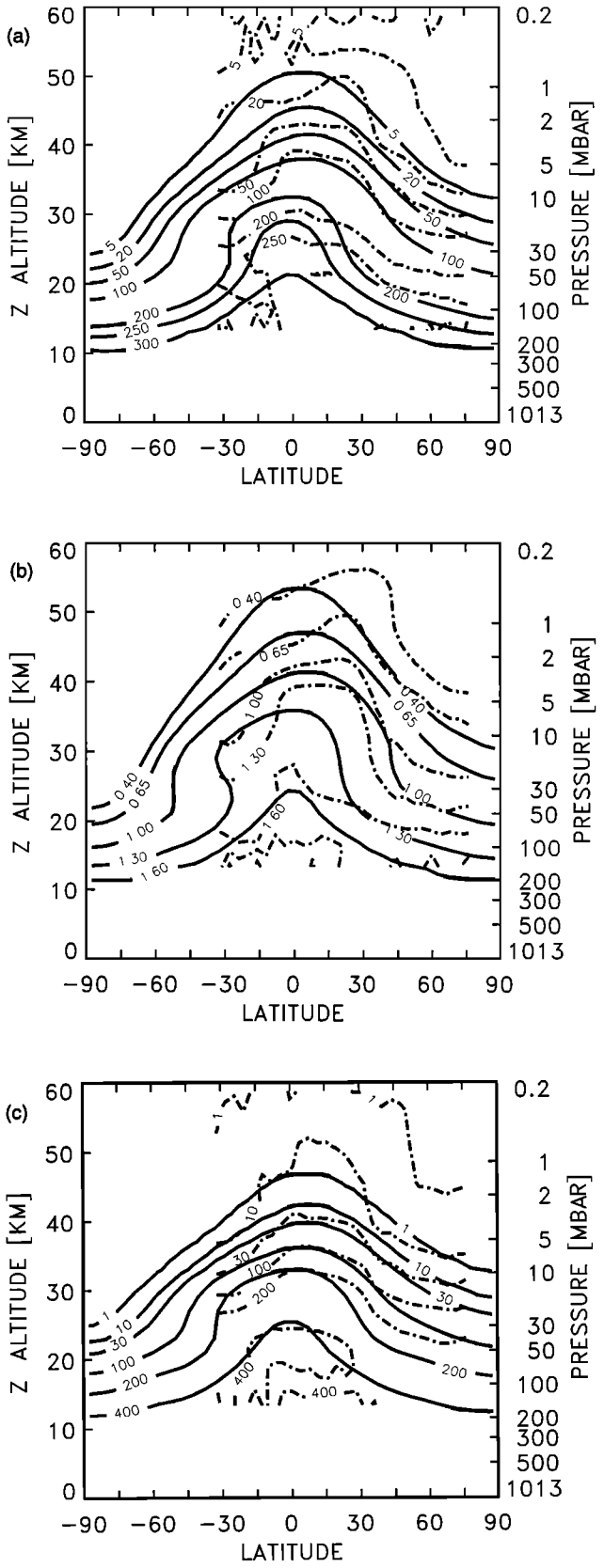

Figure 9. (a) Calculated N_2O (solid lines) and CLAES N_2O (dashed lines) for November of 1992. Units are ppb. (b) Model CH_4 (solid lines) and CLAES CH_4 (dashed lines) for November of 1992. Units are ppm. (c) Model CFC-12 (solid lines) and CLAES CFC-12 (dashed lines) for November of 1992. Units are ppm.

tudes are compared with ATMOS measurements in Figure 14. The slope of the correlation curve for midlatitudes is reproduced by the model (Figure 14a). In the tropics the model correlations between N_2O and CFC-11 for the latitude range between 5° and 15° fall below the observations except for very high N_2O (Figure 14b). If the latitude region over which the species are correlated is widened to include the whole tropics, a broad band of points is generated whose upper envelope approaches the data as shown in Figure 14c.

The discrepancy between model results and ATMOS data for the tropics may be caused by the fact that the ATMOS data consist of only one profile taken at 14° N, which is close to the northern boundary of the tropics and in a region with large latitudinal tracer gradients. Comparison of 2-D model results with data taken at a particular latitude and time is always difficult. As discussed above, the model can only represent an average year. In any particular year, the steepness and the location of the subtropical tracer gradients can vary significantly. The tracer-tracer correlations are not necessarily a more robust quantity in this case either. Correlations between two species such as N_2O and CFC-11 measured at the same location and time are necessarily compact. There is insufficient observational information to determine if these correlations are representative for the entire tropical regime. The model produces tracer gradients within the tropics which are different for the two species because of their different lifetimes. Therefore model correlations are not com-

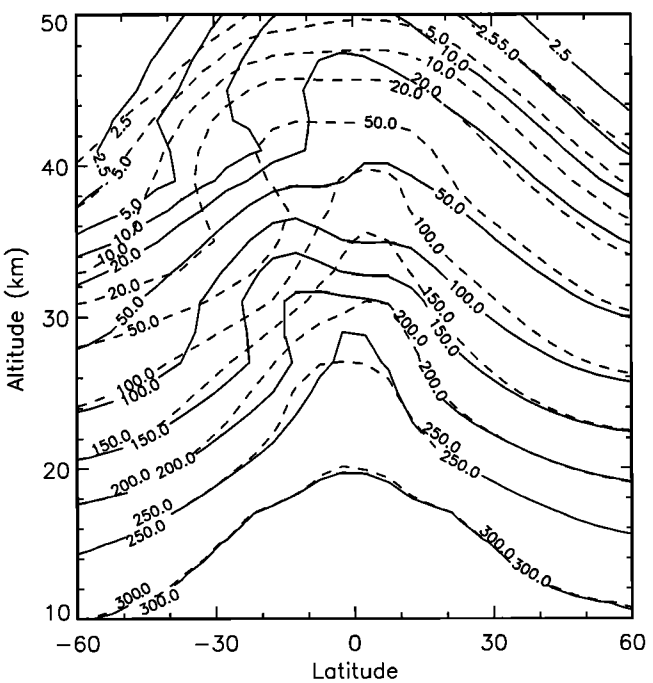

Figure 10. Stratospheric concentrations of N_2O in September for different phases of the QBO. Solid contours are for the westerly phase, and dashed contours are for the easterly phase of the QBO in the following year.

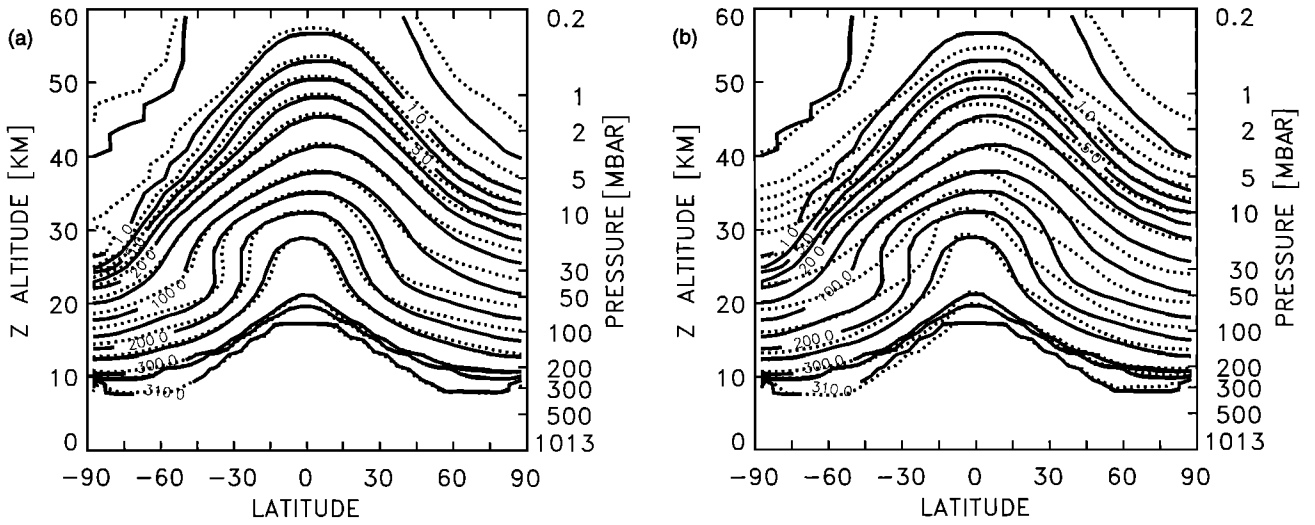

Figure 11. (a) N_2O distributions calculated for the low-K_{yy} case (solid lines) and the large-K_{yy} case (dotted lines). (b) N_2O distributions calculated for the low-K_{yy} case (solid lines) and the constant-K_{yy} case (dotted lines).

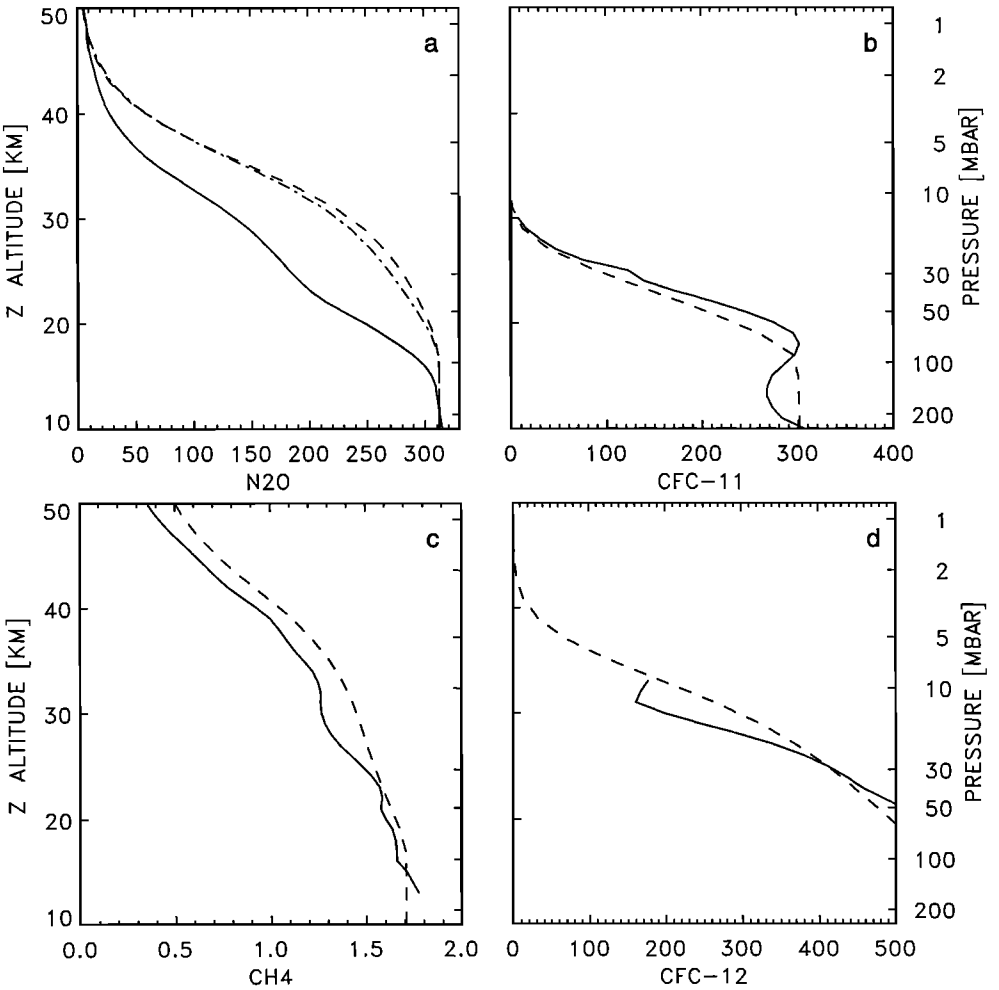

Figure 12. (a) ATMOS tropical profiles (solid line) of N_2O and model profiles, averaged between from 5° to 15° (dashed line), −10° to 10° (dash-dots) and 15° to 20° (dash-triple dots). (b) CFC-11 profile from ATMOS (solid line) and model, averaged between 5° to 15° (dashed line). (c) As in Figure 12b, but for CH_4. (d) As in Figure 12b, but for CFC-12.

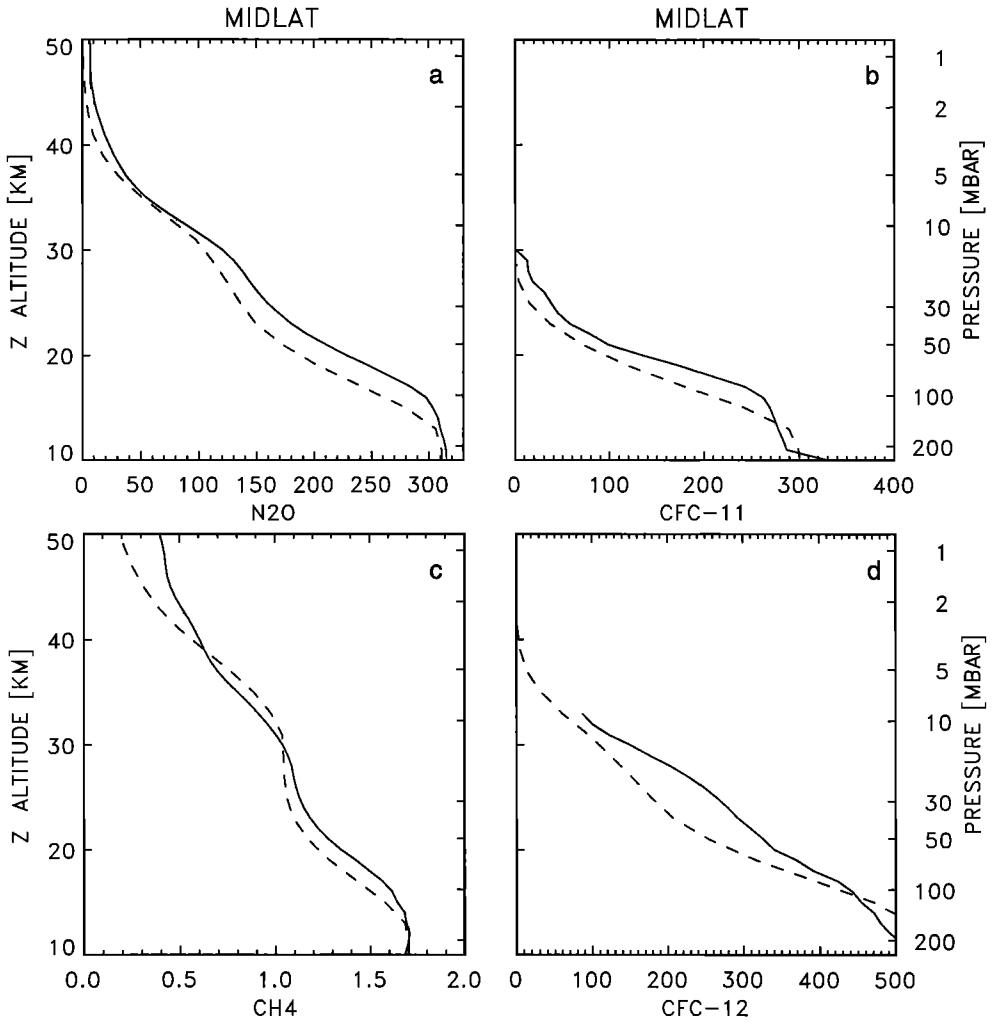

Figure 13. As Figure 12, but for midlatitudes. Profiles are averaged between 30° and 45°.

pact when evaluated across the tropics. This is further illustrated in Figure 15 which shows model cross sections of N_2O and CFC-11. In the model the isolines of those species are not parallel in the tropics and their gradients near the subtropical barrier are different. In the absense of strong horizontal diffusion in the tropics, the two tracers are not in slope equilibrium [*Plumb and Ko*, 1992].

The tropical profiles measuered by ATMOS would indicate that the upwelling in the model is too strong. Comparison with CLAES observations in the tropics for N_2O (Figure 9a) and results for mean age (see companion paper) indicate that the tropical upwelling in the model is more likely too small than too large. Therefore, in the absense of additional information for the inner tropics the ATMOS tropical profiles cannot be considered to be representative for the entire tropical regime.

5. Discussion

We have described a coupled 2-D model of the dynamics, chemistry, and radiation of stratosphere. The dynamics module is based on the transformed Eulerian mean equations and includes the nonlinear momentum advection terms in the zonal mean momentum equation. Parameterizations of effects of gravity and large-scale Rossby waves have been kept as simple as possible. Quasi-horizontal mixing has been assumed to decrease gradually from the midlatitudes to the tropics.

There is reasonable agreement between midlatitude profiles of long-lived tracers in the model and ATMOS measurements; there is good agreement also of average tropical and midlatitude profiles with the UARS data of N_2O, CH_4, and HF. In the tropics the comparison with the UARS data suggests that the strength of the upward transport in the model is more or less correct. Tropical profiles of long-lived tracers from ATMOS disagree with model profiles which may be a result of the narrow latitude region across which the data were taken and the presense of strong latitudinal gradients in the distribution of these tracers.

Subtropical gradients in the model are determined by the balance between the diffusive timescale in midlatitudes and the advective timescale in the tropics. The location and steepness of the tracer gradients is a strong

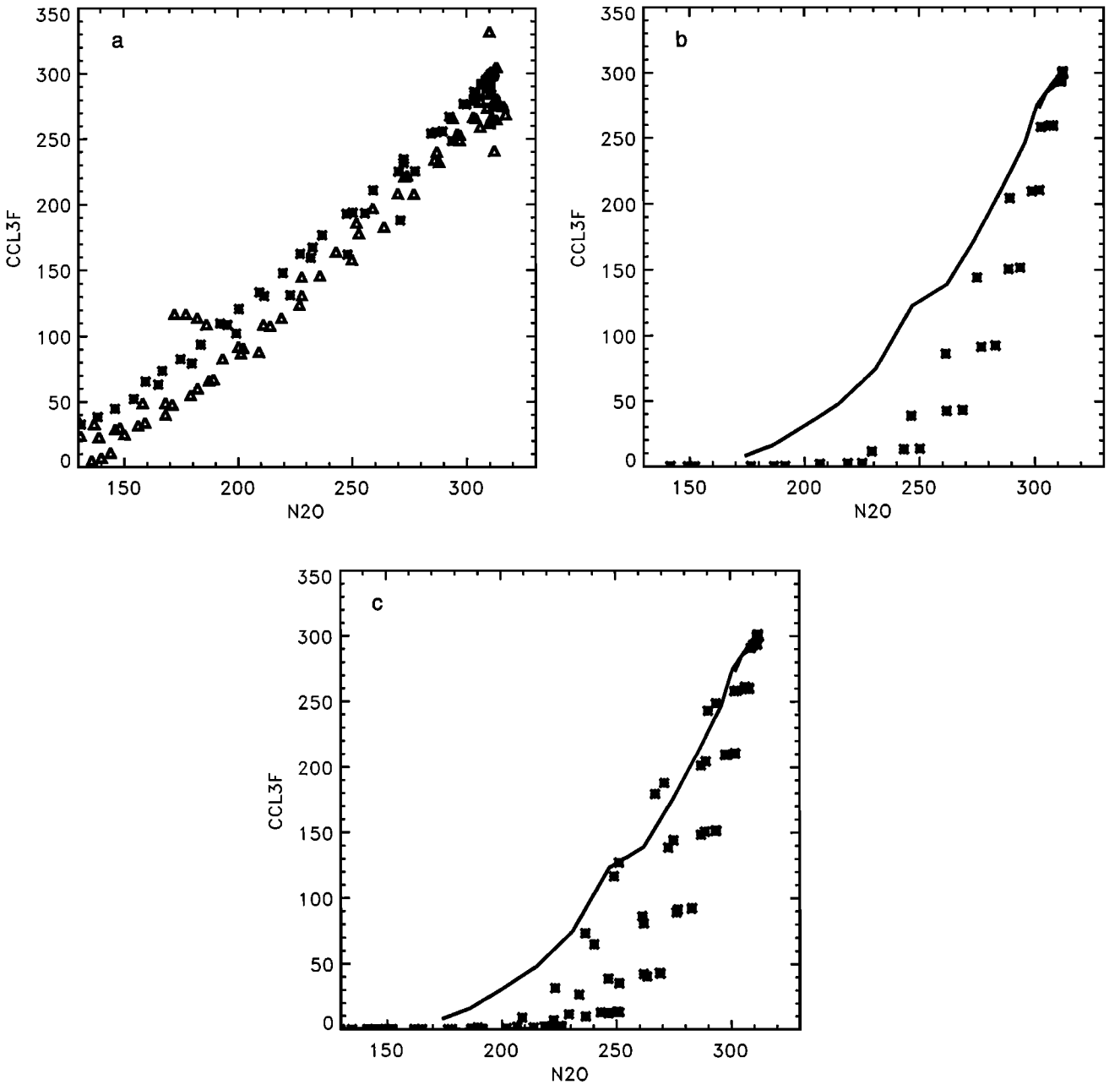

Figure 14. (a) Correlations between N_2O and CFC-11 in midlatitudes (30° to 45o). The triangles are ATMOS data, and asteriks are calculated results. (b) As in Figure 14a, but for the tropics. ATMOS data are indicated by the solid line, points are model results averaged between 5° and 15°. (c) As in Figure 14b, but model correlations for the latitude region between −10° and 20°.

function of the tropical circulation in the model. It was shown by *Jones et al.* (1998), using a version of the model that included QBO forcing terms that the modulation of tropical circulation by the QBO significantly modulates the mass exchange between tropics and midlatitudes.

Calculated temperatures disagree with observations in the polar regions of the stratosphere. The winter pole is too warm in the model and the summer pole is too cold. In addition, the tropical stratosphere is 5 K warmer than observed in the altitude region near 20 km. Mass exchange between tropics and midlatitudes is controlled by advection in the model. Advection out of the tropics and advection into the tropics, varying with season, takes place at stratospheric levels. The flow across the subtropical air mass boundary determines distributions of long-lived tracers and mean age in the lower stratosphere. Model results for CO_2 and mean age will be compared with observations in the following paper.

First sensitivity studies have been presented that show distributions of temperature and long-lived trac-

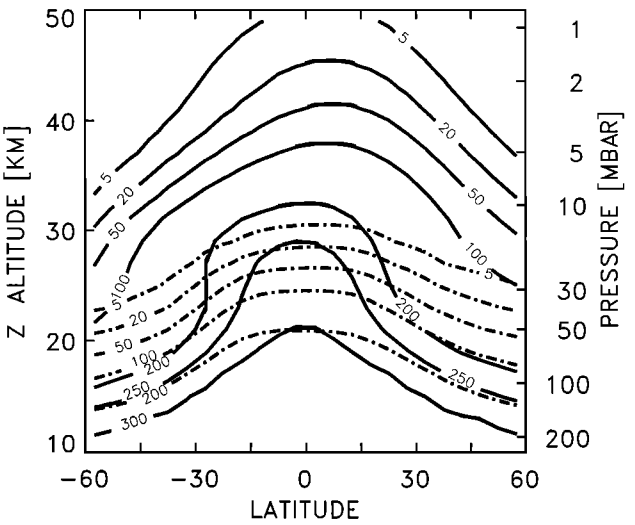

Figure 15. Cross section of model N_2O (solid lines) and model CFC-11 (dashed lines) for November.

ers being only weakly sensitive to the choice of eddy diffusion coefficients in the extratropics due to the partially compensating effects of K_{yy} on diffusive tracer transport and the circulation. Results for calculated temperatures and long-lived tracers have been shown for three different specifications of Rossby wave mixing coefficients K_{yy}. Two choices are based on the analysis of circulation data by *Newman and Schoeberl* [1986] and *Newman et al.* [1988]. These distributions assume a spatial and seasonal structure of K_{yy}. The values of the coefficients differ by a factor of 2 in the extratropics between the two cases. In addition, a control case using coefficients constant in time and in the model domain poleward of 45o has been presented.

Appendix A: Dynamics Model

The model is an updated version of the semispectral model described by *Schneider and Geller* [1985]. Versions of the zonal mean part of this model have also been used in combination with the Atmospheric and Environmental Research, In. (AER) chemistry/transport model [*Ko et al.*, 1993; *Schneider et al.*, 1993]. The zonal mean equations are given as follows.

Momentum equations

$$\begin{aligned}\partial_t\bar{u} &+ \frac{1}{\cos\Theta}\partial_y(\bar{u}\bar{v}\cos\Theta)\\ &+ \frac{1}{\rho_o}\partial_z(\rho_o\bar{u}\bar{w}^*) - f\bar{v}^*\\ &- \frac{\bar{u}\bar{v}^*}{a}\tan\Theta\\ &= -\beta\bar{u} + K_{yy}\partial_y\bar{q}, \qquad \text{(A1)}\end{aligned}$$

where $\bar{q}$ is the quasigeostrophic potential vorticity and

$$\begin{aligned}\partial_y\bar{q} &= 2\frac{\Omega}{a}\cos\Theta - \partial_y\left[\frac{1}{\cos\Theta}\partial_y(\bar{u}\cos\Theta)\right]\\ &- \frac{f^2}{N^2}\frac{1}{\rho_o}\partial_z(\rho_o\bar{u}_z)\end{aligned}$$

is the horizontal derivative of the potential vorticity.

$$\partial_t\bar{v}^* + f\bar{u} + \frac{\bar{u}^2}{a}\tan\Theta = -\partial\bar{\Phi} \qquad \text{(A2)}$$

Thermodynamic equation

$$\begin{aligned}\partial_t\bar{T} &+ \frac{1}{\cos\Theta}\partial_y(\bar{T}\bar{v}^*\cos\Theta)\\ &+ \frac{1}{\rho_o}\partial_z(\rho_o\bar{T}\bar{w}^*) + \bar{w}^*N^2\\ &+ \frac{\kappa}{H}\bar{w}^*\bar{T} = \frac{\bar{Q}}{c_p}. \qquad \text{(A3)}\end{aligned}$$

Continuity equation

$$\frac{1}{\cos\Theta}\partial_y(\bar{v}^*\cos\Theta) + \frac{1}{\rho_o}\partial_z(\rho_o\bar{w}^*) = 0. \qquad \text{(A4)}$$

In the above equations, Θ is the latitude angle $dy = a\,d\Theta$, where a is the radius of the Earth. Zonal, meridional, and vertical velocity components are denoted by u, v and w, respectively. $f = 2\Omega\sin\Theta$ is the Coriolis parameter. Log-pressure coordinates are used in the vertical:

$$z = H\ln\left(\frac{p}{p_o}\right),$$

where p is the pressure and H is the scale height, taken to be 7 km. The basic state density ρ_o is defined as

$$\rho_o = \rho_{\text{surface}}\exp(-zH).$$

The temperature

$$\bar{T} = \frac{H}{R}\partial_z\bar{\Phi}.$$

is defined as the deviation from a reference temperature profile, $T_{\text{ref}}(z)$. The values of $N^2(z)$ are the Brunt-Vaisala frequency based on the reference temperature. The deviations from the reference profile do not have to average out to zero at a given level because the term $(\kappa/H)\bar{w}^*\bar{T}$ is kept in the thermodynamic equation. The reason for defining the temperature as a deviation from a reference temperature is largely historical. It also makes it easier to restructure the model for diagnostic purposes using simplified heating schemes that cannot compute the global average heating rates.

Zonal mean winds are specified at the lower boundary (1 km). Heating rates are taken from the radiative transfer model for stratospheric altitudes and from a parameterization (see text) for the troposphere. he equations are integrated forward, using a split explicit time integration scheme. Time steps are of the order of 8 min for rapidly varying terms and 1/2 hour for slowly changing quantities.

Appendix B: Chemistry Model

The chemistry module is a newly developed family model. The version used here contains a total of 62 species. There are 25 transported species, of which three are families, and 33 equilibrium species. These

Table B1. Species Definition

	Species				
Fixed Species	N_2	O_2H_2	H_2O		
Transported Species	O_x	NO_y	Cl_y	HONO	HNO_3
	HNO_4	HN_2O_5	HCl	HOCI	$ClONO_2$
	Cl_2	$ClOOCl_3$	N_2O	CH_4	CO_2
	CO	CCl_4	CCl_3F	F_2Cl_2	CH_3Cl
	CH_3CCl_3	CHF_2Cl	CF_2O	CClFO	HF
Equilibrium Species	O	$O(^1D)$	O_3	N	NO
	NO_2	NO_3	HONO	HNO_3	HNO_4
	N_2O5	Cl	ClO	HCl	HOCl
	$ClONO_2$	ClNO	Cl_2	$ClNO_2$	ClONO
	ClOO	ClOOCl	OClO	OH	H
	HO_2	H_2O_2	HCO	CH_2O	CH_3
	CH_3 O	CH_3O_2	CH_3OOH		

species are listed in Table B1. The families are defined as follows:

$$O_x = O+O(^1D)+O_3+NO_2+ClOHO_2,$$

$$NO_y = N+NO+NO_2+NO_3+HONO+HNO_3+HNO_4 +2xN_2O_5+ClONO_2+ClNO+ClNO_2+ClONO,$$

$$Cl_y = ClClO+HCl+HOCl+ClONO_2+ClNO+2xCl_2 +ClNO_2+ClONO+ClOO+2xClOOCl+OClO,$$

$$HO_x = OH+H+HO_2+H_2O_2,$$

$$CH_x = HCO+CH_2O+CH_3+CH_3O+CH_3O_2 +CH_3OOH.$$

The tracer transport equation is solved for every long-lived species or family. However, the HO_x and CH_x families are not transported. Their definitions are used only for diagnostic purposes. Short-lived species are computed at time intervals of 5 to 10 days, assuming photochemical steady state, with an iterative Newton-Raphson method. Production terms and loss frequencies for the long-lived species are recalculated at these intervals using the updated short-lived species concentrations. Species that are long-lived in certain parts of the atmosphere are included under the long-lived and the equilibrium (short-lived) species categories. In regions where their lifetime is short, those species are determined by photochemical equilibrium, and results from the transport calculation are discarded. The reverse is done in regions where these species are long-lived. For the calculations presented here, the species of intermediate lifetimes have been treated as transported species in the polar night only.

Photochemical equilibrium is solved for 24-hour average concentrations of the short-lived species using diurnal coefficients. To calculate the diurnal coefficients, we periodically perform a full diurnal integration for 1 day. Diurnal coefficients, α and β, are then calculated using the definitions

$$\alpha = \frac{\langle C_i C_j \rangle}{\langle C_i \rangle \langle C_j \rangle},$$

$$\beta = \frac{\langle J_i C_i \rangle}{\langle J \rangle \langle C_i \rangle},$$

where angle brackets denote 24-hour averages, C_i is the concentration of species I, and J is the photolysis rate. We normally recalculate the diurnal coefficients every 10 days. However, the diurnal coefficients vary slowly in time and space and thus can be recalculated every 20 to 30 days with only small changes in the calculated abundances. The 24-hour average concentrations of the short-lived species calculated with the diurnal coefficients agree well with those calculated by the Harvard photochemical model which solves the steady state equations with exact diurnal periodicity.

For the photodissociation calculation we assume that the direct solar beam is attenuated by gas absorption and in situ Rayleigh scattering. The radiative transfer equation is solved using a six-stream approximation for clear-sky conditions in a multiple scattering atmosphere. We use the radiative transfer code from the Harvard photochemical model [*Salawitch et al.*, 1994]. The incident solar flux specified at the top of the atmosphere was taken from *World Meteorological Organization (WMO)* [1995]. Cross sections for Rayleigh scattering and for absorption in the Herzberg continuum (for wavelengths greater than 202.5 nm) of O_2 were taken from *WMO* [1995]. For absorption in the Schumann-Runge bands of O_2 we use the cross-section parameterization of *Minschwaner et al.* [1992], with the underlying Herzberg continuum included in the parameterization.

Table B2 lists the reactions used in the chemistry module. The reaction rates and absorption cross sections were all taken from *DeMore et al.* [1997], with a few exceptions. The temperature dependence of the ozone cross section between 267.5 and 342.5 nm was taken from A. M. Bass and R. J. Paur (unpublished data, 1984). We used the quantum yields for $O(^1D)$ of *Michelsen et al.* [1994]. The cross sections of NO_3 were taken from *Wayne et al.* [1991]. For wavelengths

Table B2. List of Chemical Reactions

	Reaction
k_1	$O + O_3 \rightarrow 2\times O_2$
k_2	$O(^1D) + O_2 \rightarrow O + O_2$
k_3	$O(^1D) + O_3 \rightarrow 2\times O_2$
k_4	$O(^1D) + O_3 \rightarrow O_2 + 2\times O$
k_5	$O(^1D) + H_2 \rightarrow OH + H$
k_6	$O(^1D) + H_2O \rightarrow 2\times OH$
k_7	$O(^1D) + N_2 \rightarrow O + N_2$
k_8	$O(^1D) + N_2O \rightarrow N_2 + O_2$
k_9	$O(^1D) + N_2O \rightarrow 2\times NO$
k_{10}	$O(^1D) + CH_4 \rightarrow OH + CH_3$
k_{11}	$O(^1D) + CH_4 \rightarrow H_2 + C\,H_2O$
k_{12}	$O(^1D) + CFCl_3 \rightarrow CFClO + 2\times Cl$
k_{13}	$O(^1D) + CF_2Cl_2 \rightarrow CF_2O + 2\times Cl$
k_{14}	$O(^1D) + C_2F_3Cl_3 \rightarrow CF_2O + HF + 3\times Cl + CO$
k_{15}	$O(^1D) + CF_3Br \rightarrow CF_2O + HF + Br$
k_{16}	$O(^1D) + CF_2ClBr \rightarrow CF_2O + Cl + Br$
k_{17}	$O(^1D) + CCl_4 \rightarrow 4\times Cl$
k_{18}	$O(^1D) + HCl \rightarrow Cl + OH$
k_{19}	$O(^1D) + CO_2 \rightarrow O + CO_2$
k_{20}	$H + O_3 \rightarrow OH + O_2$
k_{21}	$H + HO_2 \rightarrow 2\times OH$
k_{22}	$H + HO_2 \rightarrow H_2 + O_2$
k_{23}	$H + NO_2 \rightarrow OH + NO$
k_{24}	$O + OH \rightarrow O_2 + H$
k_{25}	$O + HO_2 \rightarrow OH + O_2$
k_{26}	$O + H_2O_2 \rightarrow OH + HO_2$
k_{27}	$O + HNO_3 \rightarrow OH + NO_3$
k_{28}	$OH + O_3 \rightarrow HO_2 + O_2$
k_{29}	$OH + OH \rightarrow H_2O + O$
k_{30}	$OH + HO_2 \rightarrow H_2O + O_2$
k_{31}	$OH + H_2O_2 \rightarrow H_2O + HO_2$
k_{32}	$OH + H_2 \rightarrow H_2O + H$
k_{33}	$HO_2 + O_3 \rightarrow OH + 2 \times O_2$
k_{34}	$HO_2 + HO_2 \rightarrow H_2O_2 + O_2$
k_{35}	$HO_2 + NO_2 \rightarrow HONO + O_2$
k_{36}	$NO_3 + HO_2 \rightarrow HNO_3 + O_2$
k_{37}	$N + O_2 \rightarrow NO + O$
k_{38}	$N + O_3 \rightarrow O_2 + NO$
k_{39}	$N + NO \rightarrow N_2 + O$
k_{40}	$N + NO_2 \rightarrow N_2O + O$
k_{41}	$O + NO_2 \rightarrow NO + O_2$
k_{42}	$O + NO_3 \rightarrow NO_2 + O_2$
k_{43}	$O + HNO_4 \rightarrow OH + NO_2 + O_2$
k_{44}	$O_3 + NO \rightarrow NO_2 + O_2$
k_{45}	$O_3 + NO_2 \rightarrow NO_3 + O_2$
k_{46}	$OH + HONO \rightarrow H_2O + NO_2$
k_{47}	$OH + HNO_4 \rightarrow H_2O + NO_2 + O_2$
k_{48}	$HO_2 + NO \rightarrow NO_2 + OH$
k_{49}	$NO + NO_3 \rightarrow 2\times NO_2$
k_{50}	$O + \rightarrow C\,H_2O + H$
k_{51}	$O + C\,H_2O \rightarrow HCO + OH$
k_{52}	$OH + CH_4 \rightarrow CH_3 + H_2O$
k_{53}	$OH + C\,H_2O \rightarrow H_2O + HCO$
k_{54}	$OH + CH_3OOH \rightarrow CH_3O_2 + H_2O$
k_{55}	$OH + CH_3OOH \rightarrow C\,H_2O + OH + H_2O$
k_{56}	$CH_3O_2 + NO \rightarrow CH_3O + NO_2$
k_{57}	$CH_3O_2 + HO_2 \rightarrow CH_3OOH + O_2$
k_{58}	$CH_3O_2 + CH_3O_2 \rightarrow 2\times CH_3O + O_2$
k_{59}	$CH_3O + O_2 \rightarrow C\,H_2O + HO_2$
k_{60}	$HCO + O_2 \rightarrow CO + HO_2$
k_{61}	$Cl + O_3 \rightarrow ClO + O_2$
k_{62}	$Cl + H_2 \rightarrow HCl + H$
k_{63}	$Cl + HO_2 \rightarrow HCl + O_2$.
k_{64}	$Cl + HO_2 \rightarrow OH + ClO$
k_{65}	$Cl + H_2O_2 \rightarrow HCl + HO_2$
k_{66}	$Cl + CH_4 \rightarrow HCl + CH_3$

Table B2. (continued)

	Reaction
k_{67}	$Cl + C\,H_2O \rightarrow HCl + HCO$
k_{68}	$Cl + ClONO_2 \rightarrow Cl_2 + NO_3$
k_{69}	$Cl + CH_3Cl \rightarrow 2\times HCl$
k_{70}	$Cl + OClO \rightarrow ClO + ClO$
k_{71}	$Cl + ClOO \rightarrow Cl_2 + O_2$
k_{72}	$Cl + ClOO \rightarrow ClO + ClO$
k_{73}	$Cl + NO_3 \rightarrow ClO + NO_2$
k_{74}	$Cl + ClNO \rightarrow NO + Cl_2$
k_{75}	$Cl + HOCl \rightarrow Cl_2 + OH$
k_{76}	$ClO + O \rightarrow Cl + O_2$
k_{77}	$ClO + OH \rightarrow HO_2 + Cl$
k_{78}	$ClO + OH \rightarrow HCl + O_2$
k_{79}	$ClO + HO_2 \rightarrow HOCl + O_2$
k_{80}	$ClO + NO \rightarrow Cl + NO_2$
k_{81}	$ClO + ClO \rightarrow ClOO + Cl$
k_{82}	$ClO + ClO \rightarrow Cl_2 + O_2$
k_{83}	$ClO + ClO \rightarrow OClO + Cl$
k_{84}	$OClO + O \rightarrow ClO + O_2$
k_{85}	$OClO + OH \rightarrow HOCl + O_2$
k_{86}	$OClO + NO \rightarrow NO_2 + ClO$
k_{87}	$OH + Cl_2 \rightarrow HOCl + Cl$
k_{88}	$O + HCl \rightarrow OH + Cl$
k_{89}	$O + HOCl \rightarrow OH + ClO$
k_{90}	$O + ClONO_2 \rightarrow ClO + NO_3$
k_{91}	$OH + HCl \rightarrow H_2O + Cl$
k_{92}	$OH + HOCl \rightarrow H_2O + ClO$
k_{93}	$OH + CH_3Cl \rightarrow H_2O + Cl$
k_{94}	$OH + CH_3CCl_3 \rightarrow H_2O + 3\times Cl$
k_{95}	$OH + ClONO_2 \rightarrow HOCl + NO_3$
k_{96}	$ClNO_2 + OH \rightarrow HOCl + NO_2$
k_{97}	$Cl + CH_3CCl_3 \rightarrow HCl + 3\times Cl$
k_{98}	$NO_2 + NO \rightarrow NO + NO_2 + O_2$
k_{99}	$NO_3 + C\,H_2O \rightarrow HNO_3 + HO_2 + CO$
k_{100}	$Br + O_3 \rightarrow BrO + O_2$
k_{101}	$Br + HO_2 \rightarrow HBr + O_2$
k_{102}	$Br + C\,H_2O \rightarrow HBr + HCO$
k_{103}	$BrO + O \rightarrow Br + O_2$
k_{104}	$BrO + HO_2 \rightarrow HOBr + O_2$
k_{105}	$BrO + NO \rightarrow Br + NO_2$
k_{106}	$BrO + ClO \rightarrow Br + OClO$
k_{107}	$BrO + ClO \rightarrow Br + ClOO$
k_{108}	$BrO + ClO \rightarrow BrCl + O_2$
k_{109}	$BrO + BrO \rightarrow 2\times Br + O_2$
k_{110}	$HBr + OH \rightarrow Br + H_2O$
k_{111}	$HBr + O \rightarrow OH + Br$
k_{112}	$HOBr + O \rightarrow OH + BrO$
k_{113}	$CH_3Br + OH \rightarrow 2\times H_2O$
k_{114}	$CHF_2Cl + OH \rightarrow CF_2O + Cl + H_2O$
k_{115}	$CHF_2Cl + Cl \rightarrow CF_2O + Cl + HCl$
k_{116}	$CHF_2Cl + O(^1D) \rightarrow CF_2O + HO_2 + Cl$
l_1	$O + O_2 \rightarrow O_3$
l_2	$O(^1D) + N_2 \rightarrow N_2O$
l_3	$H + O_2 \rightarrow HO_2$
l_4	$OH + OH \rightarrow H_2O_2$
l_5	$O + NO \rightarrow NO_2$
l_6	$O + NO_2 \rightarrow NO_3$
l_7	$OH + NO \rightarrow HONO$
l_8	$OH + NO_2 \rightarrow HNO_3$
l_9	$HO_2 + NO_2 \rightarrow HNO_4$
l_{10}	$NO_2 + NO_3 \rightarrow N_2O_5$
l_{11}	$ClO + NO_2 \rightarrow ClONO_2$
l_{12}	$CH_3 + O_2 \rightarrow CH_3O_2$
l_{13}	$ClO + ClO \rightarrow ClOOCl$
l_{14}	$Cl + NO_2 \rightarrow ClONO$
l_{15}	$Cl + NO_2 \rightarrow ClNO_2$
l_{16}	$Cl + NO \rightarrow ClNO$
l_{17}	$Cl + O_2 \rightarrow ClOO$

Table B2. (continued)

	Reaction
l_{18}	$BrO + NO_2 \rightarrow BrONO_2$
l_{19}	$N_2O_5 \rightarrow NO_2 + NO_3$
l_{20}	$HNO_4 \rightarrow HO_2 + NO_2$
l_{21}	$HO_2 + HO_2 \rightarrow H_2O_2 + O_2$
l_{22}	$OH + HNO_3 \rightarrow H_2O + NO_3$
l_{23}	$OH + CO \rightarrow H + CO_2$
l_{24}	$ClOO \rightarrow Cl + O_2$
l_{25}	$ClOOCl \rightarrow ClO + ClO$
l_{26}	$N_2O_5 \rightarrow 2\times HNO_3$
l_{27}	$ClONO_2 \rightarrow HNO_3 + HOCl$
l_{28}	$ClONO_2 + HCl \rightarrow HNO_3 + Cl2$
l_{29}	$BrONO_2 \rightarrow HNO_3 + HOBr$
l_{30}	$HOBr + HCl \rightarrow BrCl + H_2O$
l_{31}	$HOCl + HCl \rightarrow Cl2 + H_2O$
J_1	$O_2 \rightarrow 2\times O$
J_2	$O_3 \rightarrow O(^1D) + O_2$
J_3	$O_3 \rightarrow O_2 + O$
J_4	$H_2O \rightarrow OH + H$
J_5	$HO_2 \rightarrow OH + O$
J_6	$H_2O_2 \rightarrow 2\times OH$
J_7	$NO \rightarrow N + O$
J_8	$NO_2 \rightarrow NO + O$
J_9	$NO_3 \rightarrow NO + O_2$
J_{10}	$NO_3 \rightarrow NO_2 + O$
J_{11}	$N_2O \rightarrow N_2 + O(^1D)$
J_{12}	$N_2O_5 \rightarrow NO_3 + NO + O$
J_{13}	$N_2O_5 \rightarrow NO_3 + NO_2$
J_{14}	$HONO \rightarrow OH + NO$
J_{15}	$HNO_3 \rightarrow OH + NO_2$
J_{16}	$HNO_4 \rightarrow OH + NO_3$
J_{17}	$HNO_4 \rightarrow HO_2 + NO_2$
J_{18}	$ClO \rightarrow Cl + O(^1D)$
J_{19}	$ClO \rightarrow Cl + O$
J_{20}	$Cl_2 \rightarrow 2\times Cl$
J_{21}	$ClOO \rightarrow ClO + O$
J_{22}	$OClO \rightarrow ClO + O$
J_{23}	$ClOOCl \rightarrow Cl + ClOO$
J_{24}	$HCl \rightarrow H + Cl$
J_{25}	$HOCl \rightarrow OH + Cl$
J_{26}	$ClNO \rightarrow Cl + NO$
J_{27}	$ClNO_2 \rightarrow Cl + NO_2$
J_{28}	$ClONO \rightarrow Cl + NO_2$
J_{29}	$ClONO_2 \rightarrow Cl + NO_3$
J_{30}	$ClONO_2 \rightarrow ClO + NO_2$
J_{31}	$CCl_4 \rightarrow 4\times Cl$
J_{32}	$CFCl_3 \rightarrow CFClO + 2\times Cl$
J_{33}	$CF_2Cl_2 \rightarrow CF_2O + 2\times Cl$
J_{34}	$CH_3Cl \rightarrow CH_3 + Cl$
J_{35}	$CH_3CCl_3 \rightarrow 3\times Cl$
J_{36}	$C\ H_2O \rightarrow HCO + H$
J_{37}	$C\ H_2O \rightarrow CO + H_2$
J_{38}	$CH_3OOH \rightarrow CH_3O + OH$
J_{39}	$BrCl \rightarrow Br + Cl$
J_{40}	$BrO \rightarrow Br + O$
J_{41}	$HOBr \rightarrow Br + OH$
J_{42}	$BrONO_2 \rightarrow Br + NO_3$
J_{43}	$BrONO_2 \rightarrow BrO + NO_2$
J_{44}	$CH_3Br \rightarrow Br + CH_3$
J_{45}	$C_2F_3Cl_3 \rightarrow CF_2O + HF + 3\times Cl + CO$
J_{46}	$CHF_2Cl \rightarrow CF_2O + Cl$
J_{47}	$CF_3Br \rightarrow CF_2O + HF + Br$
J_{48}	$CF_2ClBr \rightarrow CF_2O + Cl + Br$
J_{49}	$CF_2O \rightarrow CO + 2\times HF$
J_{50}	$CFClO \rightarrow CO + HF + Cl$
	Total of 197 Reactions

between 200 and 280 nm we used the absorption cross sections of N_2O_5 reported by *Atkinson et al.* [1992]. The cross sections of H_2O_2, H_2O, and ClOOCl were extrapolated to longer wavelengths. For HOCl, $ClONO_2$, and CH_3OOH we used the cross sections reported by *Atkinson et al.* [1992]. The absorption cross sections of CH_2O were taken from *Atkinson et al.* [1992] for wavelengths between 240 and 300 nm. At longer wavelengths the values reported by *DeMore et al.* [1997] were used.

The concentrations of N_2, O_2, and H_2 are fixed at 78%, 21%, and 0.52 ppm, respectively. For H_2O we use an annual climatology of 2-year, monthly averages, from 1986 to 1988, from Stratospheric Aerolsol and Gas Experiment II. Surface concentrations of CO_2 are specified with monthly mean measurements of CO_2 for 1980 to 1994 obtained from T. Conway at the National Oceanic and Atmospheric Administration Climat Monitoring and Diagnostics Laboratory (personal communication, 1997). The abundance of other long-lived gases such as N_2O, CH_4, and CFCs are specified at the bottom boundary in a time-dependent fashion (see Table B3).

Table B3. Bottom Boundary Conditions for Selected Species

Species	1980 Boundary Conditions	Annual Growth Rate
N_2O, ppb	305, ppb	0.5, ppb/y
CH_4, ppm	1.6, ppm	0.005, ppm/y
CCl_3F, ppt	170, ppt	9, ppt/y
CF_2Cl_2, ppt	290, ppt	16.7, ppt/y
CH_3Cl, ppb	0.60, ppb	
CH_3CCl_3, ppt	100, ppt	6.2, ppt
CCl_4, ppt	120, ppt	1.8, ppt/y
CHF_2Cl,ppt	68.0, ppt	6.5, ppt/y
CH_3Br	0.02, ppb	0.5, ppt/y
CO, ppm	0.12, ppm	

Acknowledgments. This work was supported by DOE grant DE-F02-93ER61708, and NASA grants NAGW-1230 and NAG5-3979. Thanks are due to H. Michelsen for preparing the ATMOS data, binned by latitude, used in the comparison. T. Mergenthaler kindly supplied monthly averaged CLAES data for N_2O, CH_4, and CFC-12.

References

Andrews, D.G., and M.E. McIntyre, An exact theory of nonlinear waves on a Lagrangian Flow, *J. Fluid. Mech., 89*, 609, 1978.

Andrews, D.G., J.R. Holton, and C.B. Leovy, *Middle Atmosphere Dynamics*, 489 pp., Academic, San Diego, Calif., 1987.

Atkinson, R., D.L. Baulch, R.A.Cox, R.F. Hampson Jr., J.A. Kerr, and J. Troe, Evaluated kinetic and photochemical data for atmospheric chemistry, *J. Phys. Chem. Ref. Data, 21*, 1156, 1992.

Bachmeister, J.T., M.R. Schoeberl, M.E. Summers, J.R. Rosenfield, and X. Xhu, Descent of long-lived trace gases

in the winter polar vortex., *J. Geophys. Res., 100*, 11,669, 1995.

Cunnold, D., F. Alyea, N. Phillips, and R. Prinn, A three-dimensional dynamical-chemical model of atmospheric ozone, *J. Atmos. Sci., 32*, 170, 1975.

DeMore, W.B., et al., Chemical kinetics and photochemical data for use in stratospheric modeling, Eval. 12, *JPL Publ., 97-4*, 264 pp., 1997.

Garcia, R.R., Parameterization of planetary wave breaking in the middle atmosphere, *J. Atmos. Sci., 48*, 1405, 1991.

Holton, J.R., Meridional distribution of stratospheric trace constituents. *J. Atmos. Sci., 43*, 1238, 1986.

Holton, J.R., and W.M. Wehrbein, A numerical model of the zonal mean ciculation in the middle atmosphere, *Pure and Appl. Geophys., 118*, 284–306, 1980.

Holton, J.R., P.H. Haynes, M.E. McIntyre, A.R. Douglass, R.B. Rood, and L. Pfister, Stratosphere-troposphere exchange, *Rev. Geophys., 33*, 405, 1995.

Hou, A.Y., H.R. Schneider, and M.K.W. Ko, A dynamical explanation for the asymmetry in zonally averaged column abundances of ozone between northern and southern springs, *J. Atmos. Sci. 48*, 547, 1991.

Jones, D.B.A., H.R. Schneider, and M.B. McElroy, Effects of the quasi-biennial oscillation on the zonally averaged transport of tracers, *J. Geophys. Res., 103*, 11,235, 1998.

Ko, M.K.W., H.R. Schneider, R.-L. Shia, D. Weisenstein, and N.D. Sze, A two-dimensional model with coupled dynamics, radiation and photochemistry. 1, Simulation of the middle atmosphere, *J. Geophys. Res., 98*, 20,429, 1993.

Kogan-LeFlore, L., On the propagation of seasonally varying tracer signals into the lower stratosphere, Ph.D. thesis, Harvard Univ., Cambridge, Mass., 1999.

Krueger, A.J., and R.A. Minzner, A mid-latitude ozone model for the 1975 U. S. Standard Atmosphere, *J. Geophys. Res., 81*, 4477, 1976.

Lacis, A.A., and J.E. Hansen, A parameterization for the absorption of solar radiation in the Earth's atmosphere, *J. Atmos. Sci., 31*, 118, 1974.

Leovy, C.B., C.-R. Sun, M.H. Hitchman, E.E. Remsberg, J.M. Russel III, L.L. Gordley, J.C. Gille, and L.V. Lyjak, Transport of ozone in the middle stratosphere: Evidence for planetary wave breaking, *J. Atmos. Sci., 42*, 230, 1985.

Manney, G.L., L. Froidevaux, J.W. Waters, L.S. Elson, E.F. Fishbein, R.W. Zurek, R.S. Harwood, and W.A. Lahoz, The evolution of ozone observed by UARS MLS in the 1992 late winter southern polar vortex, *Geophys. Res. Lett., 20*, 1279, 1993.

McCormick, M.P., and R.E. Veiga, SAGE II measurements of early Pinatubo aerosols, *Geophys. Res. Lett., 19*, 155, 1992.

Michelsen, H.A., R.J. Salawitch, P.O. Wennberg, and J.G. Anderson, Production of $O(^1D)$ from photolysis of O_3, *Geophys. Res. Lett., 21*, 2227, 1994.

Minschwaner, K., G.P. Anderson, L.A. Hall, and K. Yoshino, Polynomial coefficients for calculating O_2 Schumann-Runge cross sections at 0.5 cm^{-1} resolution, *J. Geophys. Res., 97*, 10103, 1992.

Minschwaner, K., A.E. Dessler, J.W. Elkins, C.M. Volk, D.W. Fahey, M. Loewenstein, J.R. Podolke, A.E. Roche, and K.R. Chan, Bulk properties of isentropic mixing into the tropics in the lower stratosphere, *J. Geophys. Res., 101*, 9433, 1996.

Murphy, D.M., D.W. Fahey, M.H. Profitt, S.C. Liu, K.R. Chan, C.S. Eubank, S.R. Kawa, and K.K. Kelly, Reactive nitrogen and its correlation with ozone in the lower stratosphere and upper troposphere, *J. Geophys. Res., 98*, 8751, 1993.

Newman, P.A., and M.R. Schoeberl, Horizontal mixing coefficients for two-dimensional chemical models calculated from National Meteorological Center data, *J. Geophys. Res., 91*, 7919, 1986.

Newman, P.A., M.R. Schoeberl, R.A. Plumb, and J.E. Rosenfield, Mixing rates calculated from potential vorticity, *J. Geophys. Res., 93*, 5221, 1988.

Oort, A.H., Atmospheric circulation statistics, *NOAA Prof. Pap. 14*, 180 pp., U.S. Dep. of Commer., Rockville, Md., 1983.

Park, J.R. (ed.), M.K.W. Ko, C.H. Jackman, R.A. Plumb, J.A. Kaye, and K.H. Sage, Models and Measurements Intercomparison II, *NASA/TM-19999-209554*, 494 pp., Langley Research Center, Hampton, VA, 1999.

Plumb, R.A., A "tropical pipe model" of stratospheric transport, *J. Geophys. Res., 101*, 3957, 1996.

Plumb, R.A. and M.K.W. Ko, Interrelationships between mixing ratios of long-lived stratospheric constituents, *J. Geophys. Res., 97*, 10,145, 1992.

Plumb, R.A., and J.D. Mahlman, The zonally averaged transport characteristics of the GFDL general circulation/transport model, *J. Atmos. Sci., 44*, 298, 1987.

Randel, W.J., and R.R. Garcia, Application of a planetary wave breaking parameterization to stratospheric circulation statistics, *J. Atmos. Sci., 51*, 1157, 1994.

Randel, W.J., J.C. Gille, A.E. Roche, J.B. Kumer, J.L. Mergenthaler, J.W. Waters, E.F. Fishbein, and A.W. Lahoz, Stratospheric transport from the tropics to middle latitudes by planetary wave mixing, *Nature, 365*, 533, 1993.

Salawitch, R.J., et al., The distribution of hydrogen, nitrogen, and chlorine radicals in the lower stratosphere: Implications for changes in O_3 due to emission of NO_y from supersonic aircraft, *Geophys. Res. Lett., 21*, 2547, 1994.

Schneider, H.R., A numerical transport scheme which avoids negative mixing ratios, *Mon. Wea. Rev., 112*, 1206, 1984.

Schneider, H.R. and M.A. Geller, A comparison of two- and three-dimensional transport within a stratospheric circulation model, *J. Atmos. Sci., 42*, 1792, 1985.

Schneider, H.R., M.K. W.Ko, N.D. Sze, G.-Y. Shi, and W.-C. Wang, An evaluation of the role of eddy diffusion in stratospheric interactive 2-D models, *J. Atmos. Sci., 46*, 2079, 1989.

Schneider, H.R., M.K.W.Ko, R.-L. Shia, and N.D. Sze, A two-dimensional model with coupled dynamics, radiation, and photochemistry, 2, Assessment of the response of stratospheric ozone levels to increased levels of CO_2, N_2O, CH_4 and CFCs, *J. Geophys. Res., 98*, 20,441, 1993.

Schneider, H.R., D.B.A. Jones, S.C. Wopfsy, and M.B. McElroy, Analysis of residual mean transport in the stratosphere, 2, Distributions of CO_2 and mean age, *J. Geophys. Res.*, this issue.

Shi, Guang-Yu, An accurate calculation and representation of the infrared transmission function of the atmospheric constitutes, Ph.D. thesis, 191 pp., Dep. of Sci., Tohoku University of Japan, 1981.

Shi, Guang-Yu, The cooling rate due to 9.6 micrometer ozone band: A new approximation, *Sci. Sin., Series B, 27*, 947, 1984.

Trepte, C.R., and M.H. Hitchman, Tropical stratospheric circulation deduced from satellite aerosol data, *Nature*, 355, 626, 1992.

Tung, K.K., Nongeostrophic theory of zonally averaged circulation, I, Formulation, *J. Atmos. Sci., 43*, 2600, 1986.

Wayne, R.P., et al., The nitrate radical: Physics, chemistry, and the atmosphere, *Atmos. Environ., 25A*, 1, 1991.

World Meeorological Organization (WMO), Scientific Assessment of Ozone Depletion, 1994, Rept. No. 37, Geneva, Switzerland, 1995.

Wu, M.-F., M.A. Geller, J.G. Olson, and M.E. Gelman,

Troposphere-Stratosphere (surface to 55 km) monthly general circulation statistics for the Northern Hemisphere—four-year averages, NASA/TM 86182, 95 pp., Goddard Space Flight Center, Greenbelt, Maryland, 1984.

D. B. A. Jones, M. B. McElroy, and H. R. Schneider, Department of Earth and Planetary Sciences and Division of Engineering and Applied Sciences, Harvard University, 29 Oxford St., Cambridge, MA 02138. (dbj@io.harvard.edu, mbm@io.harvard.edu; hrs@io.harvard.edu)

G.-Y. Shi, Institute for Atmospheric Physics, Chinese Academy of Sciences, Beijing 100029, China. (shigy@linux2.iap.ac.cn)

(Received July 16, 1999; revised January 14, 2000; accepted March 29, 2000.)